Electronic Research Archive

https://www.aimspress.com/journal/era

ERA, 33(8): 5100–5132.
DOI: 10.3934/era.2025229
Received: 02 July 2025
Revised: 11 August 2025
Accepted: 20 August 2025
Published: 29 August 2025

Research article

Modeling and optimal control analysis of age-structured Brucellosis under environmental transmission with vaccination and culling

Qun Dai and Liming Guo*

School of Mathematics and Statistics, Changchun University of Science and Technology, Changchun 130022, China

* **Correspondence:** Email: 2023102105@mails.cust.edu.cn.

Abstract: Brucellosis is currently recognized as one of the most serious zoonotic infectious diseases, caused by *Brucella abortus*, and is classified by the World Organization for Animal Health as a Category B zoonotic disease. In this study, we developed a new seven-compartment model of the transmission dynamics brucellosis in sheep, which accounts for the combined effects of vaccination, age structure, culling of infected sheep, and the impact of the contaminated environment. Our analysis demonstrates that the DFE point of the system is globally and asymptotically stable when the basic reproduction number $R_0 < 1$. Furthermore, we show that the disease persists when $R_0 > 1$, in accordance with the theory of uniform persistence. In the numerical simulation section, we fit data on the number of Brucella infections in sheep in Egypt from 1999 to 2010 and estimate the model's parameters using the least squares method. Based on this, we propose four control strategies to establish the optimal control system. We applied Pontryagin's maximum principle to derive the necessary conditions for optimal control and perform numerical simulations. A cost-benefit analysis was conducted from the perspective of sheep farmers. Our findings suggest that the most cost-effective strategy for reducing brucellosis infection rates in sheep is to uniformly house young sheep and vaccinate them simultaneously.

Keywords: Brucellosis; vaccination; contaminated environments; uniform persistence; optimal control

1. Introduction

Brucellosis is caused by *Brucella abortus*, a small, intracellular, Gram-negative, coccoid-rod-shaped bacterium. Brucella organisms can invade the body via the digestive tract, the respiratory tract, skin, or mucous membranes. Infections are typically acquired through handling infected livestock, consumption of contaminated dairy products, or ingestion of undercooked meat

from affected animals. Sheep, cattle, and pigs are particularly susceptible to this infection. The disease presents in two stages: acute and chronic. Acute infection is characterized by symptoms such as fever and arthralgia, while chronic infection is marked by prolonged low-grade fever and fatigue. Since its discovery in 1886, brucellosis has been reported in approximately 85% of countries worldwide, with widespread outbreaks occurring, particularly in China since the 1950s [1]. However, its prevention and control pose substantial challenges: *Brucella* exhibits high resilience, with the ability to parasitize and replicate within immune cells; it can persist in the environment for extended periods; its transmission routes are diverse (encompassing the digestive tract, the respiratory tract, skin, and mucous membranes); and available vaccines have limited efficacy. Common control measures include disinfection, culling of infected animals, and vaccination, but the wide range of transmission routes complicates comprehensive prevention [1].

Against this backdrop, dynamic modeling has emerged as a powerful tool for analyzing the transmission of brucellosis. By examining the stability of these models, targeted prevention and control strategies can be formulated, providing theoretical support for disease management, especially in the agricultural and livestock sectors. Dynamic models can also predict the epidemiological trends of the disease, facilitating the development of rational prevention and control strategies.

Numerous scholars have primarily employed transmission dynamics and statistical methods to study brucellosis, with transmission dynamics being the most widely adopted approach. As early as 1994, González-Guzmán and Naulin [2] developed a dynamic model for the transmission of brucellosis in cattle, which included four compartments: Susceptible, abortion-infected, infected, and vaccinated. They provided three mathematical characterizations of the disease (outbreak, evolution, and epidemiological status) and determined the threshold for a brucellosis outbreak using singular perturbation theory.

In the application of mathematical models to analyze disease transmission patterns, proving the system's stability is essential. Through stability analysis, we can determine whether brucellosis tends to become endemic or be eradicated. Dynamic models of brucellosis have evolved from simple three-dimensional, four-dimensional, and five-dimensional systems to higher-dimensional ones. As more factors are incorporated, stability analysis becomes increasingly complex. Current research on brucellosis encompasses intra-population, inter-population, and cross-population transmission dynamics.

Studies have focused on the intra-population transmission of brucellosis. Reference [3] proves the stability of two equilibrium points by directly constructing Lyapunov functions. Reference [4] does not conduct a dynamic analysis but explores the conditions for disease elimination through a numerical simulation. Similarly, [5, 6] also prove the stability of two equilibrium points by directly constructing Lyapunov functions. The stability of the equilibrium point in [7] is proved using the comparison principle and Poincaré mapping. In [8], the Lyapunov function is used to prove the stability of the disease-free equilibrium (DFE) point, while the comparison principle and asymptotically autonomous system theory are applied to the endemic equilibrium point. Reference [9] constructs an age-structured dynamic model, uses the Hurwitz criterion to prove the local stability of the DFE point, applies center manifold theory to the endemic equilibrium point, and then constructs Lyapunov functions to prove the global stability of both equilibrium points.

Reference [10] establishes a dynamic model of sheep-human brucellosis transmission and proves the stability of two equilibrium points by constructing Lyapunov functions. The model in [11] consists

of two patch models: The stability of the DFE point is proved by directly constructing a Lyapunov function, and the stability of the two patches is verified under specific conditions. Reference [12] develops a dynamic model of cross-transmission between cattle and sheep based on mixed farming systems. It first uses the Hurwitz criterion to prove the local stability of the DFE point and then verifies its global attractivity. For the endemic equilibrium point, it confirms existence and uniqueness before constructing a Lyapunov function to prove global stability.

Aïnseba et al. [13] developed a dynamic model for sheep brucellosis that incorporates both direct and indirect transmission. The study calculates the basic reproduction number, analyzes the global system stability, and provides numerical simulations for slaughter strategies, concluding that environmental pollution plays a significant role in disease persistence and control. In 2017, Li et al. [14] established a seven-compartment human-sheep model considering environmental infection pathways, dividing the infection period into acute and chronic stages, and deriving prevention and monitoring strategies through a numerical simulation. In 2018, Meng and Abdurahman [15] expanded on Li's work by developing a six-compartment sheep model including latent and immunized populations; numerical simulations indicated that increasing disinfection frequency and improving immunization rates could effectively control transmission.

Zinsstag et al. [16] analyzed the epidemiological situation of brucellosis in Mongolia and developed a coupled human-sheep-cattle three-herd dynamics model based on actual surveillance data, predicting local epidemiological trends and proposing risk management strategies. Li et al. [17] established a coupled human-sheep herd dynamics model to analyze brucellosis trends in major Chinese provinces (e.g., Xing'anmeng and Inner Mongolia), finding that inoculation, detection, and culling effectively controlled spread.

Many scholars have incorporated age structure into their models. For example, Holt et al. [18] developed a stochastic age-structured model incorporating cattle herds' demographic data to characterize the intra- and inter-herd transmission of *Brucella abortus*. Their results suggested prioritizing vaccination of replacement heifers on large farms (considering stakeholder acceptance and vaccine supply constraints) as an effective strategy. Wang and Abdurahman [19] constructed a multi-stage deterministic model for sheep brucellosis with incomplete immunity and later developed a stochastic version incorporating ambient white noise effects on transmission, conducting a series of dynamic analyses.

Zhou et al. [20] developed a human-sheep interaction model and proposed a multi-objective optimization problem (transformed into a scalar optimization problem via the weighted sum method) aimed at minimizing the total control costs. Using Pontryagin's maximum principle, they determined the optimal control strategies, concluding that brucellosis will continue to spread in Inner Mongolia under current inadequate controls, recommending vaccination and health education as essential interventions. Nannyonga et al. [21] constructed a model assessing brucellosis susceptibility, considering direct transmission (contact with infected individuals/contaminated environments) and vertical transmission (mother to child). They performed optimal control analysis using three time-dependent measures (prevention of exposure, elimination of infected individuals, and reduction in environmental transmission) to minimize costs and infection numbers, applying Pontryagin's maximum principle.

In summary, we conclude that vaccination, age structure, and environmental contamination significantly influence the epidemiological trends of brucellosis. However, most existing models have

incorporated only one of these factors. Therefore, we propose a new model that integrates vaccination, age structure, and environmental contamination, building upon the framework of transmission dynamics outlined in existing models. Additionally, since brucellosis-infected sheep are typically culled once detected in a flock, and improper or delayed disposal of their carcasses poses a high risk of further environmental contamination, we also account for the effect of culled sheep on environmental contamination. In the numerical simulation section, we calibrate the model using data on brucellosis-infected sheep in Egypt.

The paper is organized as follows: In Section 2, we introduce a new mathematical model for brucellosis. In Section 3, we analyze the model's dynamics. Section 4 presents various control strategies and discusses the optimal control strategy. In Section 5, we calibrate the model using the least squares method, employing Egyptian brucellosis data as an example, and then analyze the cost-effectiveness. Finally, in Section 6, we discuss and summarize the conclusions.

2. Model formulation

This paper proposes a novel $S_jVS_aEIS_cW$ model with seven compartments, integrating vaccination, age structure, and environmental contamination. The total sheep population is divided into five epidemiological classes, namely susceptible juvenile sheep S_j, vaccinated individuals V, susceptible adult sheep S_a, exposed individuals E, and infected individuals I, with the total active population given by $N = S_j + V + S_a + E + I$. Additionally, S_c denotes the count of culled (inactivated) sheep, and W represents the level of environmental contamination. The schematic diagram of the model is presented in Figure 1, and the detailed parameter definitions are provided in Table 1.

$$\begin{cases} \dfrac{\mathrm{d}S_j}{\mathrm{d}t} = \Lambda - \beta_1 S_j I - \sigma_1 S_j W - (d+k+m)S_j, \\ \dfrac{\mathrm{d}V}{\mathrm{d}t} = kS_j - \beta_2 VI - \sigma_2 VW - dV, \\ \dfrac{\mathrm{d}S_a}{\mathrm{d}t} = mS_j - \beta_3 S_a I - \sigma_3 S_a W - dS_a, \\ \dfrac{\mathrm{d}E}{\mathrm{d}t} = (1-p)(\beta_1 S_j + \beta_3 S_a)I + \beta_2 VI + (1-q)(\sigma_1 S_j + \sigma_3 S_a)W + \sigma_2 VW - (d+h)E, \\ \dfrac{\mathrm{d}I}{\mathrm{d}t} = hE + p(\beta_1 S_j + \beta_3 S_a)I + q(\sigma_1 S_j + \sigma_3 S_a)W - (d+\mu+\gamma)I, \\ \dfrac{\mathrm{d}S_c}{\mathrm{d}t} = \gamma I - \eta S_c, \\ \dfrac{\mathrm{d}W}{\mathrm{d}t} = \omega_1 I + \omega_2 S_c - nW, \end{cases} \tag{2.1}$$

where k is non-negative, and all other parameters are positive.

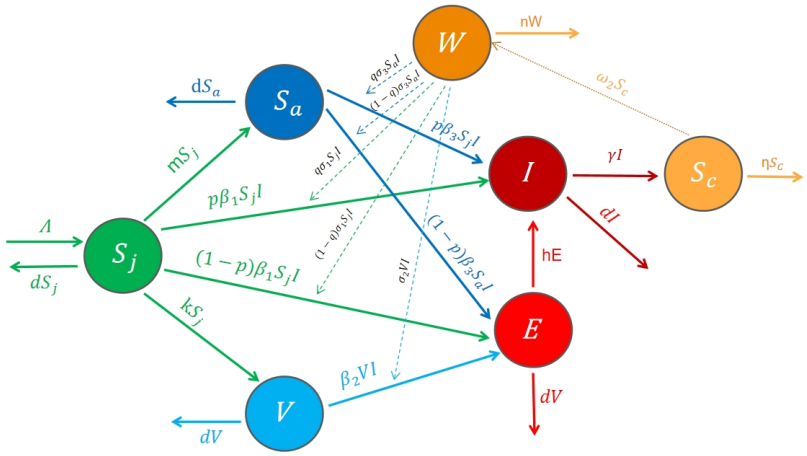

Figure 1. Flow diagram of the model.

Table 1. Meaning of the compartments and parameters in the model.

1. Meaning of each compartment	
S_j	Susceptible juvenile sheep (young sheep that are not vaccinated and are susceptible to infection)
V	Vaccinated individuals (sheep that have received vaccination)
S_a	Susceptible adult sheep (adult sheep that are not vaccinated and are susceptible to infection)
E	Exposed individuals (sheep that have been infected but are not yet infectious)
I	Infected individuals (sheep that are infected and are capable of transmitting the disease)
S_c	Inactivated sheep (sheep that have been culled or have died due to infection)
W	Contaminated environment (environment polluted by brucellosis from infected or inactivated sheep)
2. Meaning of each parameter	
Λ	Recruitment rate of sheep
d	Natural mortality of sheep
μ	Disease-related mortality in sheep
k	Vaccination coverage of sheep
m	Lambing rate
β_1	Contact rate between young susceptible sheep S_j and infected sheep I
β_2	Contact rate between vaccinated sheep V and infected sheep I
β_3	Contact rate between susceptible adult sheep S_a and infected sheep I
h	Rate of progression from exposed to infected individuals
ω_1	Rate of viral shedding in infected sheep I
γ	Inactivation rate of infected sheep I
σ_1	Exposure rate of young susceptible sheep S_j to the contaminated environment W
σ_2	Exposure rate of vaccinated sheep V to the contaminated environment W
σ_3	Exposure rate of susceptible adult sheep S_a to the contaminated environment W
ω_2	Rate of environmental contamination by the inactivated corpses of infected sheep I
η	Rate of removal of the inactivated corpses of infected sheep I
n	Virus clearance in contaminated environments
p	Proportion of symptomatic brucellosis infections due to direct transmission
q	Proportion of symptomatic brucellosis infections due to indirect transmission

3. Stability and persistence analysis

3.1. Existence and uniqueness of solutions

In the study of infectious disease models, the existence and uniqueness of solutions form the basis for ensuring the validity of model analysis. This section will utilize the Picard-Lindelöf theorem to prove that the solution of model (2.1) exists and is unique within the biologically feasible region.

To prove the existence and uniqueness of solutions for model (2.1), we employ the Picard-Lindelöf theorem [22]. First, we rewrite the model equations in vector form

$$\frac{d\mathbf{X}}{dt} = \mathbf{f}(\mathbf{X}), \tag{3.1}$$

where $\mathbf{X}(t) = \left(S_j(t), V(t), S_a(t), E(t), I(t), S_c(t), W(t)\right)^T$ and $\mathbf{f}(\mathbf{X})$ is the vector function composed of the right-hand sides of the system (2.1).

Lemma 3.1 (Picard-Lindelöf)**.** *Consider the system of ordinary differential equations* $\frac{d\mathbf{X}}{dt} = \mathbf{f}(\mathbf{X}, t)$*, where* $\mathbf{f} : D \times [t_0, t_1] \to \mathbb{R}^n$*, and* $D \subset \mathbb{R}^n$ *is an open set. If* $\mathbf{f}$ *is continuous on* $D \times [t_0, t_1]$ *and satisfies the Lipschitz condition with respect to* $\mathbf{X}$*, i.e., a constant* $L > 0$ *exists such that:*

$$\|\mathbf{f}(\mathbf{X}, t) - \mathbf{f}(\mathbf{Y}, t)\| \leq L\|\mathbf{X} - \mathbf{Y}\|, \tag{3.2}$$

for all $\mathbf{X}, \mathbf{Y} \in D$ *and* $t \in [t_0, t_1]$*. Then for any initial condition* $\mathbf{X}(t_0) = \mathbf{X}_0 \in D$*, the system has a unique solution* $\mathbf{X}(t)$ *defined on some interval containing* t_0*.*

Proof. We need to verify that model (2.1) satisfies the conditions of the Picard-Lindelöf theorem.

Each component of the function $\mathbf{f}(\mathbf{X})$ consists of polynomials and rational functions of the variables S_j, V, S_a, E, I, S_c and W. Since these functions are continuous within their domains and all variables in biological models are non-negative, $\mathbf{f}(\mathbf{X})$ is continuous in the domain $\mathbb{R}^7_+ = \{\mathbf{X} \in \mathbb{R}^7 \mid x_i \geq 0, i = 1, \ldots, 7\}$.

To verify the Lipschitz condition, we consider two arbitrary points $\mathbf{X} = (S_j, V, S_a, E, I, S_c, W)$ and $\mathbf{Y} = (\hat{S}_j, \hat{V}, \hat{S}_a, \hat{E}, \hat{I}, \hat{S}_0, \hat{W})$, and estimate $\|\mathbf{f}(\mathbf{X}) - \mathbf{f}(\mathbf{Y})\|$.

First, consider the first component of $\mathbf{f}(\mathbf{X})$

$$\begin{aligned} f_1(\mathbf{X}) - f_1(\mathbf{Y}) &= -\beta_1(S_j I - \hat{S}_j \hat{I}) - \sigma_1(S_j W - \hat{S}_j \hat{W}) - (d + k + m)(S_j - \hat{S}_j) \\ &= -\beta_1\left(S_j(I - \hat{I}) + \hat{I}(S_j - \hat{S}_j)\right) - \sigma_1\left(S_j(W - \hat{W}) + \hat{W}(S_j - \hat{S}_j)\right) - (d + k + m)(S_j - \hat{S}_j). \end{aligned}$$

Using the absolute value inequality and the triangle inequality, we obtain

$$\begin{aligned} |f_1(\mathbf{X}) - f_1(\mathbf{Y})| &\leq \beta_1|S_j||I - \hat{I}| + \beta_1|\hat{I}||S_j - \hat{S}_j| + \sigma_1|S_j||W - \hat{W}| + \sigma_1|\hat{W}||S_j - \hat{S}_j| + (d + k + m)|S_j - \hat{S}_j| \\ &\leq \beta_1 M|I - \hat{I}| + (\beta_1 M + \sigma_1 M + d + k + m)\,|S_j - \hat{S}_j| + \sigma_1 M|W - \hat{W}|, \end{aligned}$$

where M is a sufficiently large positive constant such that all variables are bounded by M within the bounded closed domain $D = \{\mathbf{X} \in \mathbb{R}^7_+ \mid 0 \leq x_i \leq M, i = 1, \ldots, 7\}$.

Similarly, for other components of $\mathbf{f}(\mathbf{X})$, we can perform an item-by-item analysis. Summarizing the estimation results of all terms, we have

$$|f_4(\mathbf{X}) - f_4(\mathbf{Y})| \leq C_{41}|S_j - \hat{S}_j| + C_{42}|V - \hat{V}| + C_{43}|S_a - \hat{S}_a| + C_{44}|E - \hat{E}| + C_{45}|I - \hat{I}| + C_{46}|S_c - \hat{S}_0| + C_{47}|W - \hat{W}|,$$

where C_{4i} are non-negative constants determined by the model parameters and M.

After conducting a similar analysis for all seven components, we can conclude that

$$\|\mathbf{f}(\mathbf{X}) - \mathbf{f}(\mathbf{Y})\|_\infty \leq L\|\mathbf{X} - \mathbf{Y}\|_\infty, \tag{3.3}$$

where $L = \max_{i=1,\ldots,7} \sum_{k=1}^{7} C_{ik}$, and C_{ik} are the Lipschitz coefficients corresponding to the i-th component with respect to the k-th variable.

Note that the functions f_i are polyno-mial functions and, therefore, smooth functions on their variables on a closed bounded set of$\mathbb{R}^7_+$. Therefore, these functions satisfy a Lipschitz condition (see [22]).

Since $\mathbf{f}(\mathbf{X})$ is continuous and satisfies the Lipschitz condition on the bounded closed domain $D \subset \mathbb{R}^7_+$, according to the Picard-Lindelöf theorem, for any initial condition $\mathbf{X}(0) \in D$, model (2.1) has a unique solution $\mathbf{X}(t)$ defined on some interval $[0, T)$ containing $t = 0$.

Further analysis shows that, in the biological context, all variables remain non-negative, and the system has a positively invariant set. Therefore, the solution can be extended to the entire time interval $[0, +\infty)$.

Theorem 3.2. *The system* (2.1) *admits a unique global non-negative solution for any non-negative initial condition.*

3.2. Positive invariant set

In what follows, we analyze the dynamical behavior of the system (2.1). First, we specify the initial conditions of the system as follows:

$$\varphi_0 = (S_j(0), V(0), S_a(0), E(0), I(0), S_c(0), W(0)) \in \mathbb{R}^{7+}.$$

Evidently, given the non-negative initial conditions, all solutions of the system remain non-negative. Furthermore, we proceed to show that the solutions are uniformly bounded.

Theorem 3.3. *The solutions of the system* (2.1) *are uniformly bounded, meaning that the solutions of the system ultimately converge to the following*

$$\Omega = \Big\{S_j(t), V(t), S_a(t), E(t), I(t), S_c(t), W(t) \in \mathbb{R}^{7+} \\ 0 \leq S_j(t) + V(t) + S_a(t) + E(t) + I(t) \leq \tfrac{\Lambda}{d}, 0 \leq S_c(t) \leq \tfrac{\gamma\Lambda}{d\eta}, 0 \leq W(t) \leq \tfrac{\max\{\omega_1,\omega_2\}\Lambda}{dn}\Big\}.$$

Proof. It is evident that $\mathbb{R}^7_+$ constitutes a positively invariant set for the system (2.1), implying that if the initial conditions lie within $\mathbb{R}^7_+$, the corresponding trajectory will remain there for all time. Consequently, $N = S_j + V + S_a + E + I \geq 0$, with $S_c \geq 0$ and $W \geq 0$ also holding. From the system (2.1), it follows that

$$\begin{aligned}\frac{\mathrm{d}N}{\mathrm{d}t} &= \Lambda - dS_j - dV - dS_a - dE - (d+\mu)I\\ &= \Lambda - (S_j + V + S_a + E + I)d - \mu I\\ &= \Lambda - Nd - \mu I\\ &\le \Lambda - dN.\end{aligned}$$

By the comparison principle, a $T > 0$ exists such that $N(t) \le \frac{\Lambda}{d}$ for all $t \ge T$. Analogously, applying the same line of reasoning to the last two equations of system (2.1) yields

$$\begin{aligned}\frac{\mathrm{d}S_c}{\mathrm{d}t} &= \gamma I - \eta S_c\\ &\le \gamma N - \eta S_c\\ &\le \frac{\gamma\Lambda}{d} - \eta S_c.\end{aligned}$$

$$\begin{aligned}\frac{\mathrm{d}W}{\mathrm{d}t} &= \omega_1 I + \omega_2 S_c - nW\\ &\le \max\{\omega_1,\omega_2\}N - nW\\ &\le \frac{\max\{\omega_1,\omega_2\}\Lambda}{d} - nW.\end{aligned}$$

Analogously, a $T > 0$ exists such that for all $t \ge T$, $W \le \frac{\max\{\omega_1,\omega_2\}\Lambda}{dn}$, $S_c \le \frac{\gamma\Lambda}{d\eta}$. In conclusion, all solutions of the system are uniformly bounded.

3.3. The basic regeneration number

We first compute the DFE of the system. Setting $E = I = 0$ immediately yields $S_c = 0$ and $W = 0$. From the first three equations of the system (2.1), we derive

$$\begin{aligned}\Lambda - (d+k+m)S_j = 0 \quad &\Longrightarrow \quad S_j = \frac{\Lambda}{d+k+m},\\ k\frac{\Lambda}{d+k+m} - dV = 0 \quad &\Longrightarrow \quad V = \frac{k\Lambda}{d(d+k+m)},\\ m\frac{\Lambda}{d+k+m} - dS_a = 0 \quad &\Longrightarrow \quad S_a = \frac{m\Lambda}{d(d+k+m)}.\end{aligned} \tag{3.4}$$

From this, we derive the DFE of the system as follows:

$$E_0\left(\frac{\Lambda}{d+k+m}, \frac{k\Lambda}{d(d+k+m)}, \frac{m\Lambda}{d(d+k+m)}, 0, 0, 0\right). \tag{3.5}$$

Next, following the formulation of the basic reproduction number provided in [23, 24], we utilize the next-generation matrix method to derive the basic reproduction number for the disease. According to the framework introduced by van den Driessche and Watmough in [24], the matrices **F** and **V**—which represent the new infection terms and the remaining transition terms, respectively—are defined as follows:

$$\mathcal{F} = \begin{pmatrix} (1-p)\beta_1 S_j I + (1-p)\beta_3 S_a I + \beta_2 V I + (1-q)\sigma_1 S_j W + (1-q)\sigma_3 S_a W + \sigma_2 V W \\ p\beta_1 S_j I + p\beta_3 S_a I + q\sigma_1 S_j W + q\sigma_3 S_a W \\ 0 \\ 0 \end{pmatrix}, \tag{3.6}$$

$$\mathcal{V} = \begin{pmatrix} (d+h)\,E \\ -hE + (d+\mu+\gamma)\,I \\ -\gamma I + \eta S_c \\ -\omega_1 I - \omega_2 S_c + mW \end{pmatrix}. \tag{3.7}$$

The partial derivatives of the aforementioned matrices are computed below. These derivatives are essential for constructing the Jacobian matrix of the system evaluated at DFE.

$$F = \begin{pmatrix} 0 & (1-p)\beta_1 S_j{}^0 + (1-p)\beta_3 S_a{}^0 + \beta_2 V^0 & 0 & (1-q)\sigma_1 S_j{}^0 + (1-q)\sigma_3 S_a{}^0 + \sigma_2 V^0 \\ 0 & p\beta_1 S_j{}^0 + p\beta_3 S_a{}^0 & 0 & q\sigma_1 S_j{}^0 + q\sigma_3 S_a{}^0 \\ 0 & 0 & 0 & 0 \\ 0 & 0 & 0 & 0 \end{pmatrix}, \tag{3.8}$$

$$V = \begin{pmatrix} d+h & 0 & 0 & 0 \\ -h & d+\mu+\gamma & 0 & 0 \\ 0 & -\gamma & \eta & 0 \\ 0 & -\omega_1 & -\omega_2 & 0 \end{pmatrix}. \tag{3.9}$$

The basic reproduction number is given by $\rho(FV^{-1})$, and is thus expressed as

$$R_0 = R_1 + R_2, \tag{3.10}$$

where

$$R_1 = \frac{[(1-p)\beta_1 S_j{}^0 + (1-p)\beta_3 S_a{}^0 + \beta_2 V^0]h + [p\beta_1 S_j{}^0 + p\beta_3 S_a{}^0]f_1}{f_1 f_2}, \tag{3.11}$$

$$R_2 = \frac{\eta\omega_1 + \gamma\omega_2}{n\eta} \frac{[(1-q)\sigma_1 S_j{}^0 + (1-q)\sigma_3 S_a{}^0 + \sigma_2 V^0]h + [q\sigma_1 S_j{}^0 + q\sigma_3 S_a{}^0]f_1}{f_1 f_2}, \tag{3.12}$$

where $f_1 = d + h$, $f_2 = d + \mu + \gamma$, R_1 denotes the average number of secondary infections generated via direct transmission from infected individuals, and R_2 represents the average number of individuals indirectly infected by viruses shed into the environment by infected individuals.

3.4. Stability of disease-free equilibrium points

In this subsection, we analyze the local and global asymptotic stability of the DFE.

Theorem 3.4. *When $R_0 < 1$, the system* (2.1) *is locally asymptotically stable at the DFE point E_0. When $R_0 > 1$, the system* (2.1) *becomes unstable at the DFE point E_0.*

Proof. First, we linearize the system (2.1) at the DFE E_0. The Jacobian matrix $J(E_0)$ evaluated at the DFE is expressed follows:

$$\begin{pmatrix} -(d+k+m) & 0 & 0 & 0 & -\beta_1 S_j{}^0 & 0 & -\sigma_1 S_j{}^0 \\ k & -d & 0 & 0 & -\beta_2 V^0 & 0 & -\sigma_2 V^0 \\ m & 0 & -d & 0 & -\beta_3 S_a{}^0 & 0 & -\sigma_3 S_a{}^0 \\ 0 & 0 & 0 & -(d+h) & X_1 & 0 & X_3 \\ 0 & 0 & 0 & h & X_2 - f_2 & 0 & X_4 \\ 0 & 0 & 0 & 0 & \gamma & -\eta & 0 \\ 0 & 0 & 0 & 0 & \omega_1 & \omega_2 & -n \end{pmatrix},$$

where

$$\begin{aligned} X_1 &= (1-p)\beta_1 S_j{}^0 + (1-p)\beta_3 S_a{}^0 + \beta_2 V^0, \\ X_2 &= p\beta_1 S_j{}^0 + p\beta_3 S_a{}^0, \\ X_3 &= (1-q)\sigma_1 S_j{}^0 + (1-q)\sigma_3 S_a{}^0 + \sigma_2 V^0, \\ X_4 &= q\sigma_1 S_j{}^0 + q\sigma_3 S_a{}^0. \end{aligned} \tag{3.13}$$

Recall that $J(E_0) = \begin{pmatrix} A & C \\ 0 & B \end{pmatrix}$, where

$$\begin{aligned} A &= \begin{pmatrix} -(d+k+m) & 0 & 0 \\ k & -d & 0 \\ m & 0 & -d \end{pmatrix}, \mathrm{C} = \begin{pmatrix} 0 & -\beta_1 S_j{}^0 & 0 & -\sigma_1 S_j{}^0 \\ 0 & -\beta_2 V^0 & 0 & -\sigma_2 V^0 \\ 0 & -\beta_3 S_a{}^0 & 0 & -\sigma_3 S_a{}^0 \end{pmatrix}, \\ B &= \begin{pmatrix} -(d+h) & X_1 & 0 & X_3. \\ h & X_2 - f_2 & 0 & X_4 \\ 0 & \gamma & -\eta & 0 \\ 0 & \omega_1 & \omega_2 & -n \end{pmatrix}, \end{aligned} \tag{3.14}$$

then

$$|\lambda I - J(E_0)| = \begin{pmatrix} \lambda I - A & -C \\ 0 & \lambda I - B \end{pmatrix} = |\lambda I - A|\,|\lambda I - B|,$$

$$\begin{aligned} |\lambda I - A| &= \begin{vmatrix} \lambda + (d+k+m) & 0 & 0 \\ -k & \lambda + d & 0 \\ -m & 0 & \lambda + d \end{vmatrix} \\ &= [\lambda + (d+k+m)]\,(\lambda + d)(\lambda + d). \end{aligned}$$

Hence, $\lambda_1 = -(d+k+m)$, $\lambda_2 = \lambda_3 = -d$.

$$|\lambda I - B| = \begin{pmatrix} \lambda + (d+h) & -X_1 & 0 & -X_3 \\ -h & \lambda - X_2 + f_2 & 0 & -X_4 \\ 0 & -\gamma & \lambda + \eta & 0 \\ 0 & -\omega_1 & -\omega_2 & \lambda + n \end{pmatrix} = 0.$$

After simplification, we obtain

$$\begin{aligned} &(\lambda + f_1)(\lambda + f_2)(\lambda + \eta)(\lambda + n) = (\lambda + f_1)(\lambda + \eta)(\lambda + n)X_2 + (\lambda + \eta)(\lambda + n)X_1 h \\ &+X_4\omega_1(\lambda + f_1)(\lambda + \eta) + X_3\omega_1 h(\lambda + n) + X_4\gamma\omega_2(\lambda + f_1) + X_3 h\gamma\omega_2. \end{aligned}$$

In what follows, we employ the contradiction method to prove that all eigenvalues of $J(E_0)$ have negative real parts. Suppose at least one eigenvalue λ_a exists such that $\mathbf{Re}(\lambda_a) \geq 0$. In this case,

$$\begin{aligned}
1 &= \left| \begin{array}{l} \frac{X_2}{\lambda_a+f_2} + \frac{X_1 h}{(\lambda_a+f_1)(\lambda_a+f_2)} + \frac{X_4\omega_1}{(\lambda_a+f_2)(\lambda_a+n)} + \frac{X_4\gamma\omega_2}{(\lambda_a+f_2)(\lambda_a+\eta)(\lambda_a+n)} \\ + \frac{X_3 h\gamma\omega_2}{(\lambda_a+f_1)(\lambda_a+f_2)(\lambda_a+\eta)(\lambda_a+n)} + \frac{X_3\omega_1 h}{(\lambda_a+f_1)(\lambda_a+f_2)(\lambda_a+n)} \end{array} \right| \\
&\leq \frac{X_2}{f_2} + \frac{X_1 h}{f_1 f_2} + \frac{X_4\omega_1}{f_2 n} + \frac{X_4\gamma\omega_2}{f_2\eta n} + \frac{X_3 h\gamma\omega_2}{f_1 f_2\eta n} + \frac{X_3\omega_1 h}{f_1 f_2 n} \\
&= \frac{X_1 h + X_2 f_1}{f_1 f_2} + \frac{\eta\omega_1 + \gamma\omega_2}{n\eta}\frac{X_3 h + X_4 f_1}{f_1 f_2} \\
&= R_1 + R_2 \\
&= R_0.
\end{aligned}$$

This contradicts the condition $R_0 < 1$, so the assumption is invalid. Therefore, all eigenvalues of $J(E_0)$ must have negative real parts.

Theorem 3.5. *The system* (2.1) *is globally asymptotically stable at the DFE point E_0 when $R_0 \leq 1$.*

Proof. Following the construction approach of the positive-definite Lyapunov functions commonly used in similar epidemic models , we introduce the following Lyapunov function:

$$\begin{aligned}
L = hE + f_1 I + \frac{\omega_2 h[(1-q)\sigma_1 S_j{}^0 + (1-q)\sigma_3 S_a{}^0 + \sigma_2 V^0] + \omega_2 f_1[q\sigma_1 S_j{}^0 + q\sigma_3 S_a{}^0]}{n\eta} S_c \\
+ \frac{h[(1-q)\sigma_1 S_j{}^0 + (1-q)\sigma_3 S_a{}^0 + \sigma_2 V^0] + f_1[q\sigma_1 S_j{}^0 + q\sigma_3 S_a{}^0]}{n} W.
\end{aligned} \tag{3.15}$$

For notational simplicity, we introduce the following symbols:

$$\begin{aligned}
y_1 &= \frac{\omega_2 h[(1-q)\sigma_1 S_j{}^0 + (1-q)\sigma_3 S_a{}^0 + \sigma_2 V^0] + \omega_2 f_1[q\sigma_1 S_j{}^0 + q\sigma_3 S_a{}^0]}{n\eta}, \\
y_2 &= \frac{h[(1-q)\sigma_1 S_j{}^0 + (1-q)\sigma_3 S_a{}^0 + \sigma_2 V^0] + f_1[q\sigma_1 S_j{}^0 + q\sigma_3 S_a{}^0]}{n}.
\end{aligned} \tag{3.16}$$

The selection of this functional form is motivated by its ability to capture the system's key epidemiological characteristics. Specifically, the coefficients are chosen such that the time derivative $\frac{dL}{dt}$ along system trajectories satisfies

$$\begin{aligned}
\dot{L} &= h\Big[(1-p)(\beta_1 S_j + \beta_3 S_a)I + \beta_2 VI + (1-q)(\sigma_1 S_j + \sigma_3 S_a)W + \sigma_2 VW - (d+h)E\Big] \\
&\quad + f_1\Big[hE + p(\beta_1 S_j + \beta_3 S_a)I + q(\sigma_1 S_j + \sigma_3 S_a)W - (d+\mu+\gamma)I\Big] \\
&\quad + y_1(\gamma I - \eta S_c) + y_2(\omega_1 I + \omega_2 S_c - nW) \\
&\leq h\Big[(1-p)(\beta_1 S_j{}^0 + \beta_3 S_a{}^0)I + \beta_2 VI + (1-q)(\sigma_1 S_j{}^0 + \sigma_3 S_a{}^0)W + \sigma_2 V^0 W - (d+h)E\Big] \\
&\quad + f_1\Big[hE + p(\beta_1 S_j{}^0 + \beta_3 S_a{}^0)I + q(\sigma_1 S_j + \sigma_3 S_a)W - (d+\mu+\gamma)I\Big] \\
&\quad + y_1(\gamma I - \eta S_c) + y_2(\omega_1 I + \omega_2 S_c - nW)
\end{aligned}$$

$$
\begin{aligned}
&= h[X_1 I + X_3 W - f_1 E] + f_1[hE + X_2 I + X_4 W - f_2 I] \\
&\quad + y_1(\gamma I - \eta S_c) + y_2(\omega_1 I + \omega_2 S_c - nW) \\
&= (hX_1 + f_1 X_2 - f_1 f_2 - \gamma y_1 + \omega_1 y_2) I + (-h f_1 + f_1 h) E \\
&\quad + (-y_1 \eta + \omega_2 y_2) S_c + (hX_3 + f_1 X_4 - n y_2) W \\
&= (hX_1 + f_1 X_2 - f_1 f_2 - \gamma \frac{\omega_2 h X_3 + \omega_2 f_1 X_4}{n\eta} + \omega_1 \frac{hX_3 + f_1 X_4}{n}) I \\
&= f_1 f_2 \left(\frac{X_1 h + X_2 f_1}{f_1 f_2} + \frac{\eta\omega_1 + \gamma\omega_2}{n\eta} \frac{X_3 h + X_4 f_1}{f_1 f_2} - 1 \right) I \\
&= f_1 f_2 (R_1 + R_2 - 1) I \\
&= f_1 f_2 (R_0 - 1) I.
\end{aligned}
$$

Since all parameters of the system (2.1) are positive, we immediately deduce that $\dot{L} \leq 0$ when $R_0 < 1$. It follows that the maximal compact invariant subset of $\{(S_j, V, S_a, E, I, S_c, W) \in \Omega : \dot{L} = 0\}$ is the singleton $\{E_0\}$. By the LaSalle invariance principle [25], every solution of the system (2.1) with the initial conditions in Ω converges to E_0 as $t \to +\infty$ whenever $R_0 \leq 1$. Therefore, the system (2.1) is globally asymptotically stable at the DFE E_0 when $R_0 \leq 1$.

3.5. Existence of endemic equilibrium

An endemic equilibrium (EE) is defined as an equilibrium state of the system where the infection-related variables are non-zero. At the EE, all differential equations equal zero, i.e.

$$
\begin{aligned}
&\Lambda = (\beta_1 I^* + \sigma_1 W^* + d + k + m) S_j^*, \\
&k S_j^* = (\beta_2 I^* + \sigma_2 W^* + d) V^*, \\
&m S_j^* = (\beta_3 I^* + \sigma_3 W^* + d) S_a^*, \\
&\lambda_E^* = (d + h) E^*, \\
&hE^* + \lambda_I^* = (d + \mu + \gamma) I^*, \\
&\gamma I^* = \eta S_c^*, \\
&\omega_1 I^* + \omega_2 S_c^* = n W^*,
\end{aligned}
$$

where,

$$
\begin{aligned}
&\lambda_E^* = (1 - p)(\beta_1 S_j + \beta_3 S_a) I + \beta_2 V I + (1 - q)(\sigma_1 S_j + \sigma_3 S_a) W + \sigma_2 V W, \\
&\lambda_I^* = p(\beta_1 S_j + \beta_3 S_a) I + q(\sigma_1 S_j + \sigma_3 S_a) W.
\end{aligned} \tag{3.17}
$$

We write

$$
f_1 = d + h, \quad f_2 = d + \mu + \gamma, \quad c = \frac{\eta\omega_1 + \gamma\omega_2}{n\eta}. \tag{3.18}
$$

From $\frac{dS_c}{dt} = 0$, we have

$$
\gamma I^* = \eta S_c^*,
$$

$$S_c^* = \frac{\gamma}{\eta} I^*.$$

From the equation for $\frac{dW}{dt}$, we obtain

$$\omega_1 I^* + \omega_2 S_c^* = nW^*,$$

$$W^* = \frac{\omega_1 I^* + \omega_2 \cdot \frac{\gamma}{\eta} I^*}{n} = \frac{\eta\omega_1 + \gamma\omega_2}{n\eta} I^* = cI^*.$$

From the equation for $\frac{dE}{dt}$, we have

$$(1-p)(\beta_1 S_j^* + \beta_3 S_a^*) I^* + \beta_2 V^* I^* + (1-q)(\sigma_1 S_j^* + \sigma_3 S_a^*) W^* + \sigma_2 V^* W^* = (d+h)E^*.$$

Substituting $W^* = cI^*$ and dividing both sides by I^* ($I^* \neq 0$), we get

$$E^* = \frac{I^*}{f_1}\left[(1-p)(\beta_1 S_j^* + \beta_3 S_a^*) + \beta_2 V^* + (1-q)(\sigma_1 S_j^* + \sigma_3 S_a^*)c + \sigma_2 V^* c\right].$$

From the equation for $\frac{dS_j}{dt} = 0$, we derive

$$\Lambda = (\beta_1 I^* + \sigma_1 W^* + d + k + m) S_j^*,$$

$$S_j^* = \frac{\Lambda}{d + k + m + (\beta_1 + \sigma_1 c) I^*}.$$

From the equation for $\frac{dV}{dt} = 0$, we obtain

$$kS_j^* = (\beta_2 I^* + \sigma_2 W^* + d) V^*,$$

$$V^* = \frac{kS_j^*}{d + (\beta_2 + \sigma_2 c) I^*}.$$

From the equation for $\frac{dS_a}{dt} = 0$, we have

$$mS_j^* = (\beta_3 I^* + \sigma_3 W^* + d) S_a^*,$$

$$S_a^* = \frac{mS_j^*}{d + (\beta_3 + \sigma_3 c) I^*}.$$

Thus far, we have obtained the following expressions of $S_j^*, V^*, S_a^*, E^*, S_c^*, W^*$ in terms of I^*

$$\begin{aligned}
S_j^* &= \frac{\Lambda}{d + k + m + (\beta_1 + \sigma_1 c) I^*}, \\
V^* &= \frac{kS_j^*}{d + (\beta_2 + \sigma_2 c) I^*}, \\
S_a^* &= \frac{mS_j^*}{d + (\beta_3 + \sigma_3 c) I^*}, \\
E^* &= \frac{I^*}{f_1}\left[(1-p)(\beta_1 S_j^* + \beta_3 S_a^*) + \beta_2 V^* + (1-q)(\sigma_1 S_j^* + \sigma_3 S_a^*)c + \sigma_2 V^* c\right], \\
W^* &= \frac{\eta\omega_1 + \gamma\omega_2}{n\eta} I^* = cI^*, \\
S_c^* &= \frac{\gamma}{\eta} I^*.
\end{aligned} \tag{3.19}$$

To prove the existence of an EE, it suffices to show that $I^* > 0$.

From the equation for $\frac{dI}{dt} = 0$, we have

$$hE^* + p(\beta_1 S_j^* + \beta_3 S_a^*)I^* + q(\sigma_1 S_j^* + \sigma_3 S_a^*)W^* + \sigma_2 V^* W^* = f_2 I^*.$$

Substituting E^* and $W^* = cI^*$, dividing both sides by I^*, and rearranging terms, we obtain

$$\begin{aligned} F(I^*) = \frac{h}{f_1}\left[(1-p)(\beta_1 S_j^* + \beta_3 S_a^*) + \beta_2 V^* + (1-q)(\sigma_1 S_j^* + \sigma_3 S_a^*)c + \sigma_2 V^* c\right] \\ + p(\beta_1 S_j^* + \beta_3 S_a^*) + q(\sigma_1 S_j^* + \sigma_3 S_a^*)c + \sigma_2 V^* c - f_2 = 0, \end{aligned}$$

where $F(I^*) = 0$ is an equation in I^*. Note that S_j^*, V^* and S_a^* are all continuous and monotonically decreasing functions of I^*.

When $I^* = 0$, we have $S_j^* = S_j^0$, $V^* = V^0$, and $S_a^* = S_a^0$. Substituting these into $F(I^*)$ yields

$$F(0) = f_2(R_0 - 1).$$

When $R_0 > 1$, $F(0) > 0$.

As $I^* \to \infty$, $S_j^*, V^*, S_a^* \to 0$, so all terms involving S_j^*, V^*, S_a^* in $F(I^*)$ vanish, leaving only $-f_2$

$$F(I^*) \to -f_2 < 0.$$

Clearly, $F(I^*)$ is continuous on $[0, \infty)$, with

- $F(0) > 0$ (when $R_0 > 1$);
- $F(I^*) \to -\infty$ (as $I^* \to \infty$).

Therefore, a unique $I^* > 0$ exists such that $F(I^*) = 0$. Substituting this I^* into the expressions for $S_j^*, V^*, S_a^*, E^*, S_c^*$ and W^* gives an EE point with all positive variables. Hence, when $R_0 > 1$, the system has a unique EE.

Theorem 3.6. *When $R_0 > 1$, the system admits a unique EE.*

3.6. Uniformity and permanence

We now state a theorem regarding the uniform persistence of the system.

Theorem 3.7. *When $R_0 > 1$, the system described by the Eq* (2.1) *is uniformly persistent.*

To prove this theorem, we first present the following lemma.

Lemma 3.8. *[26] Suppose that*

(1) Let X be a metric space, $X_0 \subset X$ be an open set, and define $\partial X_0 := X \backslash X_0$ (where ∂X_0 need not be the topological boundary of X_0, following the standard notation in persistence theory). Let $f : X \to X$ be a continuous map satisfying $f(X_0) \subset X_0$, and let A be the global attractor of f (i.e., a nonempty, compact, invariant set that attracts every point in X).

(2) Let $M_\partial := \{x \in \partial X_0 : f^n(x) \in \partial X_0 \text{ for all } n \geq 0\}$ (the set of points in ∂X_0 whose positive orbits remain in ∂X_0). Let $A_\partial = A \cap M_\partial$ be the maximal compact invariant set of f in ∂X_0 (which may be empty). Suppose A_∂ admits a Morse decomposition $\{M_1, \cdots, M_k\}$ (a sequence of disjoint, compact, invariant subsets) with the following properties:

(a) *Each M_i is isolated in X (i.e., M_i is the maximal invariant set in some neighborhood of itself).*

(b) *For each $1 \le i \le k$, the stable set $W^s(M_i) := \{x \in X : \lim_{n\to\infty} d(f^n(x), M_i) = 0\}$ satisfies $W^s(M_i) \cap X_0 = \emptyset$.*

Then, $\delta > 0$ exists that for any compact internally chain transitive set L (a compact invariant set where, for any $a, b \in L$ and $\epsilon > 0$, there is a finite ϵ-chain connecting a and b within L) with $L \nsubseteq M_i$ for all $1 \le i \le k$, we have $\inf_{x\in L} d(x, \partial X_0) > \delta$. In other words, $f : X \to X$ is uniformly persistent with respect to $(X_0, \partial X_0)$.

Proof. Let us examine Condition 1. First, we define

$$X = \{(S_j, V, S_a, E, I, S_c, W) \in \Omega\},$$
$$X_0 = \{(S_j, V, S_a, E, I, S_c, W) \in X : E > 0, I > 0, S_c > 0, W > 0\}.$$

It is evident that

$$\partial X_0 = X \backslash X_0.$$

It is straightforward to observe that for the system (2.1), both X and X_0 are positively invariant sets, and X_0 is a closed subset of X. This implies $f(X_0) \subset X_0$. Next, we consider the global attractor A of f. By Theorem 3.1, the trajectories of the system are uniformly bounded, which guarantees the existence of at least one global attractor A for f. Thus, Condition (1) is satisfied. We now proceed to verify Condition (2), where we take

$$\begin{aligned} A_\partial = &\{(S_j(0), V(0), S_a(0), E(0), I(0), S_c(0), W(0)) \in \partial X_0 : \\ &(S_j(t), V(t), S_a(t), E(t), I(t), S_c(t), W(t)) \in \partial X_0, \forall t \ge 0\}. \end{aligned}$$

We proceed to prove this result as follows:

$$A_\partial = A_\partial^{'} = \{(S_j, V, S_a, 0, 0, 0, 0) \in \partial X : S \ge 0, V \ge 0\}.$$

It is evident that $A'_\partial \subseteq A_\partial$. We next show that $A_\partial \subseteq A'_\partial$. We use a proof by contradiction, supposing that $A_\partial \subseteq A'_\partial$ does not hold. Let $\varphi(t)$ be a solution to the system with the initial condition $\varphi(0)$ that is one-to-one, satisfying

$$\varphi(t) = (S_j(t), V(t), S_a(0), E(t), I(t), S_c(t), W(t)) \in A_\partial, \varphi(t) \notin A_\partial^{'}.$$

Then, at least one of $E(0)$, $I(0)$, $S_c(0)$, or $W(0)$ is non-zero. Without loss of generality, suppose $E(0) = 0$, $I(0) = 0$, $S_c(0) = 0$, and $W(0) > 0$. From the system (2.1), t exists such that the following

equation holds:

$$\begin{aligned}
E(t) &= e^{-f_1 t}[E(0) + \int_0^t [(1-p)(\beta_1 S_j(u) + \beta_3 S_a(u))I(u) + \beta_2 V(u)I(u) \\
&\quad (1-q)(\sigma_1 S_j(u) + \sigma_3 S_a(u))W(u) + \sigma_2 V(u)W(u)]e^{f_1 t}du] > 0, \\
I(t) &= e^{-(f_2 t - \int_0^t p(\beta_1 S_j(u) + \beta_3 S_a(u))du)}[I(0) + \int_0^t [hE(u) + q(\sigma_1 S_j(u) + \sigma_3 S_a(u))W(u) \\
&\quad e^{(f_2 u - \int_0^u p(\beta_1 S_j(h) + \beta_3 S_a(h))dh)}]du] > 0, \\
S_c(t) &= e^{-\eta t}[S_c(0) + \int_0^t \gamma I(u)e^{\eta u}du] > 0, \\
W(t) &= e^{-nt}[W(0) + \int_0^t (\omega_1 I(u) + \omega_2 S_c(u))e^{nu}du] > 0.
\end{aligned}$$

This implies the existence of some t such that $\varphi(t) \notin \partial X_0$, hence $\varphi(t) \notin \partial A_\partial$, contradicting the assumption $\varphi(t) \in \partial A_\partial$. Therefore, $A_\partial = A'_\partial$. It follows that A_∂ contains only the DFE m E_0, which is evidently isolated and invariant. We now verify Condition (b) of Lemma 2, namely $W^s(E_0) \cap X_0 = \varnothing$. By the Lyapunov stability theorem, $\varepsilon > 0$ exists such that for any solution $\Phi_t(\varphi(0))$ with the initial conditions $\varphi(0) \in X_0$, the following holds:

$$D(\Phi_t(\varphi(0)), E_0)^\infty \geq \varepsilon_1,$$

We proceed by proof of contradiction, assuming that the above conclusion is false. Specifically, for any $\varepsilon_1 > 0$, we have

$$D(\Phi_t(\varphi(0)), E_0)^\infty < \varepsilon_1.$$

This means that $T > 0$ exists such that for all $t > T$, both

$$\begin{gathered}
\frac{\Lambda}{d+k+m} - \varepsilon_1 \leq S_j(t) \leq \frac{\Lambda}{d+k+m} + \varepsilon_1, \\
\frac{k\Lambda}{d(d+k+m)} - \varepsilon_1 \leq V(t) \leq \frac{k\Lambda}{d(d+k+m)} + \varepsilon_1, \\
\frac{m\Lambda}{d(d+k+m)} - \varepsilon_1 \leq S_a(t) \leq \frac{m\Lambda}{d(d+k+m)} + \varepsilon_1, \\
0 \leq E(t) \leq \varepsilon_1, 0 \leq I(t) \leq \varepsilon_1, \quad 0 \leq S_c(t) \leq \varepsilon_1, \quad 0 \leq W(t) \leq \varepsilon_1.
\end{gathered}$$

For $t > T$, consider the following subsystem:

$$\begin{cases}
\dfrac{\mathrm{d}E}{\mathrm{d}t} = A_1(\varepsilon_1)I + A_2(\varepsilon_1)W - (d+h)E, \\
\dfrac{\mathrm{d}I}{\mathrm{d}t} = A_3(\varepsilon_1)I + A_4(\varepsilon_1)W + hE - (d+\mu+\gamma)I, \\
\dfrac{dS_c}{dt} = \gamma I - nS_c, \\
\dfrac{\mathrm{d}W}{\mathrm{d}t} = \omega_1 I + \omega_2 S_c - \eta W,
\end{cases} \tag{3.20}$$

where

$$\begin{aligned} A_1(\varepsilon_1) &= (1-p)[\beta_1(S_j^0-\varepsilon_1)+\beta_3(S_a^0-\varepsilon_1)]I+\beta_2(V^0-\varepsilon_1),\\ A_2(\varepsilon_1) &= (1-q)[\sigma_1(S_j^0-\varepsilon_1)+\sigma_3(S_a^0-\varepsilon_1)]+\sigma_2(V^0-\varepsilon_1),\\ A_3(\varepsilon_1) &= p[\beta_1(S_j^0-\varepsilon_1)+\beta_3(S_a^0-\varepsilon_1)],\\ A_4(\varepsilon_1) &= q[\sigma_1(S_j^0-\varepsilon_1)+\sigma_3(S_a^0-\varepsilon_1)]. \end{aligned} \tag{3.21}$$

We define

$$\frac{\mathrm{d}f}{\mathrm{d}t} = A(\varepsilon_1)f, \tag{3.22}$$

where

$$A(\varepsilon_1) = \begin{pmatrix} -(d+h) & A_1(\varepsilon_1) & 0 & A_2(\varepsilon_1)\\ h & A_3(\varepsilon_1)-(d+\mu+\gamma) & 0 & A_4(\varepsilon_1)\\ 0 & \gamma & -\eta & 0\\ 0 & \omega_1 & \omega_2 & -n \end{pmatrix}.$$

Recall that $S(A(\boldsymbol{\varepsilon}_1)) = \max\{\mathbf{Re}\,\lambda : \lambda \text{ is an eigenvalue of } A(\boldsymbol{\varepsilon}_1)\}$. According to the Perron-Frobenius Theorem [27], since $A(\boldsymbol{\varepsilon}_1)$ is irreducible and non-negative with non-negative diagonal entries, $S(A(\boldsymbol{\varepsilon}_1))$ corresponds to a simple eigenvalue of $A(\boldsymbol{\varepsilon}_1)$ with a positive eigenvector. From the proofs of Lemma 2.1 in [28], Theorem 2 in [24], and our previously established Theorem 2.2, we deduce that for $R_0 > 1$, we have

$$S(A(0)) > 0.$$

Since $S(A(\boldsymbol{\varepsilon}_1))$ is a continuous function of $\boldsymbol{\varepsilon}_1$, sufficiently small $\boldsymbol{\varepsilon}_1$ exists such that $S(A(\boldsymbol{\varepsilon}_1)) > 0$. Consider the solution $f(t) = (f_1(t), f_2(t), f_3(t))^T$ to the the system (2.1). As $t \to +\infty$, we have $f_i(t) \to +\infty$ for $i = 1, 2, 3$. Applying the comparison principle, we conclude that

$$\lim_{t\to+\infty} E(t) = +\infty, \lim_{t\to+\infty} I(t) = +\infty, \lim_{t\to+\infty} S_c(t) = +\infty, \lim_{t\to+\infty} W(t) = +\infty.$$

This contradiction establishes that $W^s(E_0) \cap X_0 = \varnothing$, and $\varepsilon > 0$ exists. Having verified all the hypotheses of Lemma 3.5, we conclude that the solutions of the system (2.1) are uniformly persistent when $R_0 > 1$.

4. Optimal control problem

In the preceding section, we derived the basic reproduction number R_0, which governs the disease's extinction, and analyzed the stability and persistence of the system (2.1). However, the current epidemiological trends indicate that the disease control objectives will not be achieved within the next decade. As highlighted in relevant reports, brucellosis remains a global concern due to factors such as high direct contact rates between free-range sheep and other flocks, inadequate vaccine coverage, and delayed remediation of virus-contaminated environments. Consequently, in the subsequent section, we introduce four control variables $u_1(t), u_2(t), u_3(t), u_4(t)$ to facilitate effective control of brucellosis.

The control variable $u_1(t)$ indicates the confinement of young sheep to reduce their contact with external sheep and contaminated environments, $u_2(t)$ indicates that immunized adult sheep should be isolated from external sheep to avoid contact, $u_3(t)$ corresponds to increasing the vaccination rate of young sheep, and $u_4(t)$ represents enhanced virus clearance in contaminated environments—specifically, the timely removal of contaminated environments and the carcasses of infected sheep that have been culled. On the basis of these assumptions, we present the following controlled model in this section

$$\begin{cases} \dfrac{dS_j}{dt} = \Lambda - (1-u_1)\beta_1 S_j I - (1-u_1)\sigma_1 S_j W - (1+u_3)kS_j - (d+m)S_j, \\ \dfrac{dV}{dt} = (1+u_3)kS_j - (1-u_2)\beta_2 VI - \sigma_2 VW - dV, \\ \dfrac{dS_a}{dt} = mS_j - (1-u_2)\beta_3 S_a I - \sigma_3 S_a W - dS_a, \\ \dfrac{dE}{dt} = (1-p)(1-u_1)\beta_1 S_j I + (1-p)(1-u_2)\beta_3 S_a I + (1-u_2)\beta_2 VI \\ +(1-q)(1-u_1)\sigma_1 S_j W + (1-q)\sigma_3 S_a W + \sigma_2 VW - (d+h)E, \\ \dfrac{dI}{dt} = hE + (1-u_1)p\beta_1 S_j I + p(1-u_2)\beta_3 S_a I + q(1-u_1)\sigma_1 S_j W + q\sigma_3 S_a W - (d+\mu+\gamma)I, \\ \dfrac{dS_c}{dt} = \gamma I - (1+u_4)\eta S_c, \\ \dfrac{dW}{dt} = \omega_1 I + \omega_2 S_c - (1+u_4)nW. \end{cases} \tag{4.1}$$

Next, consider the set of control variables S_j, S_a, V, E, I, S_c and W, which depend on the state variables $u(t) = (u_1(t), u_2(t), u_3(t), u_4(t)) \in U_{\text{ad}}$. The admissible control set U_{ad} is formally defined as

$$U_{\text{ad}} = \{(u_1, u_2, u_3, u_4) \mid 0 \le u_i \le 1,\ t \in [0, T_0],\ i = 1, 2, 3, 4, \text{ and } u_i(t) \text{ is Lebesgue measurable on } [0, T_0]\},$$

where U (control region) refers to the range constraint $[0, 1]$ for each control variable, and U_{ad} further incorporates the measurability condition of control variables over the time interval.

The objective is to minimize the following cost functional:

$$\begin{aligned} J(u_1(t), u_2(t), u_3(t), u_4(t)) = \int_0^{T_0} \Big(& Z_1 E(t) + Z_2 I(t) + \frac{1}{2}\xi_1 u_1^2(t) + \frac{1}{2}\xi_2 u_2^2(t) \\ & + \frac{1}{2}\xi_3 u_3^2(t) + \frac{1}{2}\xi_4 u_4^2(t) \Big) \mathrm{d}t, \end{aligned} \tag{4.2}$$

where Z_1 and Z_2 are the weighting constants for the latent and infected individuals, respectively, and $\xi_1, \xi_2, \xi_3, \xi_4$ are the weight constants corresponding to the four control variables. The objective is to find an optimal set of controls $(u_1^*(t), u_2^*(t), u_3^*(t), u_4^*(t))$ that minimizes the control cost, the number of latent individuals, and the number of infected individuals. Specifically, we aim to satisfy the condition

$$J(u_1^*(t), u_2^*(t), u_3^*(t), u_4^*(t)) = \min_{u_i \in U_{ad}} J(u_1(t), u_2(t), u_3(t), u_4(t)).$$

In the following, we first estimate the costs associated with the four control strategies. Given the lack of prior literature supporting these assumptions, we adopt the perspective of sheep farmers to derive the cost estimates.

First, consider the cost of the control strategy u_1, which involves confining young sheep to minimize their contact with external flocks and contaminated environments. This strategy is relatively straightforward for farmers to implement, as it requires only minimal additional feed for young sheep (which are too small for early free-ranging). Thus, we assume the cost of u_1 to be \$2 per sheep per year.

Next, u_2 denotes the strategy of isolating immunized adult sheep from external flocks. This is more challenging for farmers, as it necessitates additional forage for adult sheep and incurs substantial labor costs due to restricted free-ranging. Therefore, we assume the cost of u_2 to be \$35 per sheep per year.

As u_3 represents the vaccination rate of young sheep (with the goal of increasing this rate), the brucellosis vaccine is priced at approximately \$4.50. Consequently, we assume the cost associated with u_3 to be \$4.50 per sheep per year.

Finally, u_4 represents enhanced virus removal from contaminated environments. We estimate the cost of this control strategy to be \$0.5 per sheep per year.

Thus, we set $\xi_1 = 2, \xi_2 = 35, \xi_3 = 4.5$, and $\xi_4 = 0.5$.

Applying Pontryagin's maximum principle, we can express the corresponding Hamiltonian function as follows:

$$\begin{aligned} H = {} & Z_1E(t) + Z_2I(t) + \frac{1}{2}\xi_1u_1^2(t) + \frac{1}{2}\xi_2u_2^2(t) + \frac{1}{2}\xi_3u_3^2(t) + \frac{1}{2}\xi_4u_4^2(t) \\ & + \lambda_1\frac{\mathrm{d}S_j}{\mathrm{d}t} + \lambda_2\frac{\mathrm{d}V}{\mathrm{d}t} + \lambda_3\frac{\mathrm{d}S_a}{\mathrm{d}t} + \lambda_4\frac{\mathrm{d}E}{\mathrm{d}t} + \lambda_5\frac{\mathrm{d}I}{\mathrm{d}t} + \lambda_6\frac{\mathrm{d}S_c}{\mathrm{d}t} + \lambda_7\frac{\mathrm{d}W}{\mathrm{d}t}, \end{aligned} \tag{4.3}$$

where λ_i $(i = 1, 2, \ldots, 7)$ are the associated costate parameters.

In accordance with Pontryagin's maximum principle, we observe that

$$\begin{gathered} \frac{\mathrm{d}\lambda_1}{\mathrm{d}t} = -\frac{\partial H}{\partial S_j}, \quad \frac{\mathrm{d}\lambda_2}{\mathrm{d}t} = -\frac{\partial H}{\partial V}, \quad \frac{\mathrm{d}\lambda_3}{\mathrm{d}t} = -\frac{\partial H}{\partial S_a}, \quad \frac{\mathrm{d}\lambda_4}{\mathrm{d}t} = -\frac{\partial H}{\partial E}, \\ \frac{\mathrm{d}\lambda_5}{\mathrm{d}t} = -\frac{\partial H}{\partial I}, \quad \frac{\mathrm{d}\lambda_6}{\mathrm{d}t} = -\frac{\partial H}{\partial S_c}, \quad \frac{\mathrm{d}\lambda_7}{\mathrm{d}t} = -\frac{\partial H}{\partial W}. \end{gathered}$$

Hence,

$$
\begin{cases}
\dfrac{\mathrm{d}\lambda_1}{\mathrm{d}t} = \lambda_1[(1-u_1)\beta_1 I + (1-u_1)\sigma_1 W + (1+u_3)k + (d+m)] - \lambda_3 m - \lambda_2(1+u_3)k \\
\qquad\qquad - \lambda_4[(1-p)(1-u_1)\beta_1 I + (1-q)(1-u_1)\sigma_1 W] \\
\qquad\qquad - \lambda_5[(1-u_1)p\beta_1 I + q(1-u_1)\sigma_1], \\
\dfrac{\mathrm{d}\lambda_2}{\mathrm{d}t} = \lambda_2[(1-u_2)\beta_2 I + \sigma_2 W + d] - \lambda_4[(1-u_2)\beta_2 I + \sigma_2 W], \\
\dfrac{\mathrm{d}\lambda_3}{\mathrm{d}t} = \lambda_2[(1-u_2)\beta_3 I + \sigma_3 W + d] - \lambda_4[(1-p)(1-u_2)\beta_3 I + (1-q)\sigma_3 W] \\
\qquad\qquad - \lambda_5[p(1-u_2)\beta_3 I + q\sigma_3 W], \\
\dfrac{\mathrm{d}\lambda_4}{\mathrm{d}t} = -Z_1 + \lambda_4(d+h) - \lambda_5 h, \\
\dfrac{\mathrm{d}\lambda_5}{\mathrm{d}t} = -Z_2 + \lambda_1(1-u_1)\beta_1 S_j + \lambda_2(1-u_2)\beta_2 V + \lambda_3(1-u_2)\beta_3 S_a \\
\qquad\qquad - \lambda_4[(1-p)(1-u_1)\beta_1 S_j + (1-p)(1-u_2)\beta_3 S_a + (1-u_2)\beta_2 V] \\
\qquad\qquad - \lambda_5[(1-u_1)p\beta_1 S_j + p(1-u_2)\beta_3 S_a - (d+\mu+\gamma)] - \lambda_6\gamma - \lambda_7\omega_1, \\
\dfrac{\mathrm{d}\lambda_6}{\mathrm{d}t} = -\lambda_7\omega_2 + \lambda_6(1+u_4)\eta, \\
\dfrac{\mathrm{d}\lambda_7}{\mathrm{d}t} = \lambda_1(1-u_1)\sigma_1 S_j + \lambda_2\sigma_2 V + \lambda_3\sigma_3 S_a \\
\qquad\qquad - \lambda_4[(1-q)(1-u_1)\sigma_1 S_j + (1-q)\sigma_3 S_a + \sigma_2 V] \\
\qquad\qquad - \lambda_5[q(1-u_1)\sigma_1 S_j + q\sigma_3 S_a] + \lambda_7(1+u_4)n.
\end{cases}
\tag{4.4}
$$

Since the state variables of the controlled system do not have specified terminal values, the transversality conditions hold at the final time T_0

$$\lambda_i(T_0) = 0 \quad (i = 1, 2, \ldots, 7).$$

According to Pontryagin's maximum principle, the optimal control variables $u_1^*(t), u_2^*(t), u_3^*(t)$ and $u_4^*(t)$ satisfy $\frac{\partial H(t,x,u,\lambda)}{\partial u_i} = 0$ and are constrained by $0 \le u_i \le 1$ for $i = 1, 2, 3, 4$. Therefore, the optimal controls are characterized as follows:

$$u_i^* = \min\{\max\{u_{ii}, 0\}, 1\},$$

where

$$
\begin{aligned}
u_{11} &= \frac{[\lambda_4(1-p) + \lambda_5 p - \lambda_1]\beta_1 {S_j}^* I^* + [\lambda_4(1-q) + \lambda_5 q - \lambda_1]\sigma_1 {S_j}^* W^*}{\xi_1}, \\
u_{22} &= \frac{[\lambda_4 - \lambda_2]\beta_2 V^* I^* + [\lambda_4(1-p) + \lambda_5 p - \lambda_3]\beta_3 {S_a}^* I^*}{\xi_2}, \\
u_{33} &= \frac{(\lambda_1 - \lambda_2)k{S_j}^*}{\xi_3}, \\
u_{44} &= \frac{\lambda_6\eta {S_c}^* + \lambda_7 n W^*}{\xi_4},
\end{aligned}
\tag{4.5}
$$

where $S_j^*, V^*, S_a^*, I^*, S_c^*, W^*$ is the optimal solution obtained in by solving, on each iteration, problem with the boundary conditions and $\lambda_i, i = 1...7$ is the adjoint function.

5. Model calibration

In this subsection, we first fixed certain parameters by referring to relevant literature [10, 17, 29, 30] and then estimated the remaining parameters using the least squares method. The estimation was based on the brucellosis prevalence data of Egyptian sheep from January 1999 to December 2010, as reported in the General Veterinary Organization's report [31]. The total number of annual brucellosis infections in sheep was calculated using the total population of Egyptian sheep and the prevalence rate.

We employed a weighted least squares approach to minimize the mean squared errors (MSEs) between the observed data and the model's predictions. The dataset used in this study was extracted from the brucellosis prevalence records of Egyptian sheep, as reported by the General Veterinary Organization, spanning from January 1999 to December 2010. Specifically, we minimized the following MSE function:

$$\text{MSE} = \sum_{i=1}^{N} \frac{(x(t_i) - X_i)^2}{N}, \tag{5.1}$$

where X_i denotes the observed data values, and $x(t_i)$ represents the model-predicted values at the exact time points t_i corresponding to the observed data. This method ensures that

$$x(t_i) = I(t_i). \tag{5.2}$$

As noted in [31], the number of test animals in that study was consistently very small relative to the total size of Egypt's animal population. Moreover, since no sampling plan was provided, sampling bias cannot be ruled out. Therefore, we preprocessed the data as follows: the positive rate detected in 2009, which contained obvious errors, was replaced with the average of the positive rates detected in 2008 and 2010. The relevant specific data are presented in Table 2, and the specific parameter values can be found in Table 3.

The fit of the model (2.1) to the brucellosis prevalence data in Egypt from January 1999 to 2010 is shown in Figure 2, where the purple points represent the actual observed data, and the blue curves denote the model-predicted outcomes.

Due to the significant difficulty in obtaining data on brucellosis in sheep, we only found data on brucellosis infections in Egyptian sheep from 1999 to 2010, which were used to calibrate the model. To demonstrate the predictive ability of the calibrated model for the period 2011–2025, we refer to the summary of the actual brucellosis prevalence published by the Egyptian government, as reported in [32]. As can be observed from Figure 3, the trend changes between 2010 and 2025 are roughly consistent with those predicted by our model, which indirectly validates the predictive capacity of our model.

Table 2. Number of Brucellosis cases in Egypt, January 1999–2010.

Years	Total for Egypt	Number of tests	Number of positives	Rate of infection	Total number of infections
1999	4,390,730	62,151	1437	2.31	1,014,263
2000	4,469,130	68,342	1303	1.91	85,360
2001	4,671,240	78,310	1967	2.51	117,248
2002	5,105,000	99,466	1111	1.12	57,176
2003	4,939,000	79,565	1755	2.21	109,152
2004	5,043,000	68,122	1081	1.59	80,184
2005	5,232,000	69,571	1203	1.73	90,514
2006	5,385,000	71,929	905	1.26	67,851
2007	5,467,470	68,171	924	1.36	74,358
2008	5,498,030	106,215	968	0.91	50,032
2009	5,591,850	84,798	3095	0.85	47,531
2010	5,529,530	66,412	525	0.79	43,683

Table 3. Values for each parameter of the model.

Parameters	Parameter value	Unit	Source
Λ	946,292	sheep/year	Fitted
d	0.25	1/year	[31]
μ	0.15	1/year	[10]
k	0.316	1/year	[10]
m	1.06	1/year	[31]
β_1	1.56×10^{-6}	1/(sheep·year)	Fitted
β_2	5.4×10^{-5}	1/(sheep·year)	Fitted
β_3	2.58×10^{-6}	1/(sheep·year)	Fitted
ω_1	16	1/year	[31]
γ	0.09	1/year	Fitted
σ_1	3.6×10^{-11}	1/(sheep·year)	Fitted
σ_2	4.7×10^{-8}	1/(sheep·year)	Fitted
σ_3	2.47×10^{-10}	1/(sheep·year)	Fitted
ω_2	16	1/year	[31]
η	0.14	1/year	Fitted
h	1.64×10^{-5}	1/year	Fitted
n	0.1	1/year	Fitted
p	0.1	Unitless	Assumed
q	0.2	Unitless	Assumed

Using the parameter values in Table 3, we calculate the basic reproduction number $R_0 = 1.56$, which exceeds unity. This result indicates that, in the absence of control measures, brucellosis will persist

endemically in Egypt and will not naturally vanish.

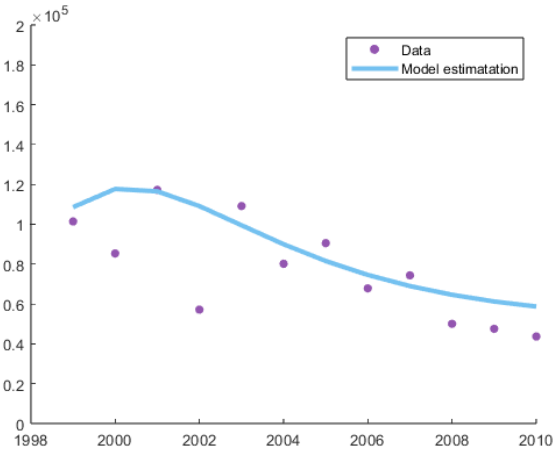

Figure 2. Model calibration of brucellosis infection cases in Egypt.

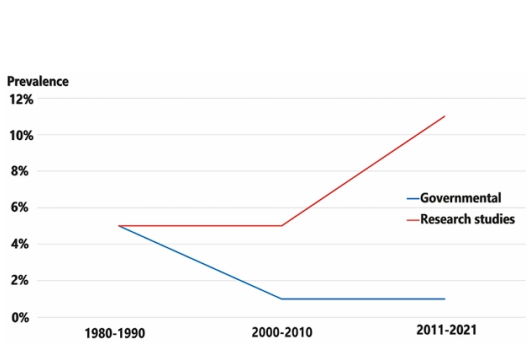

(a)

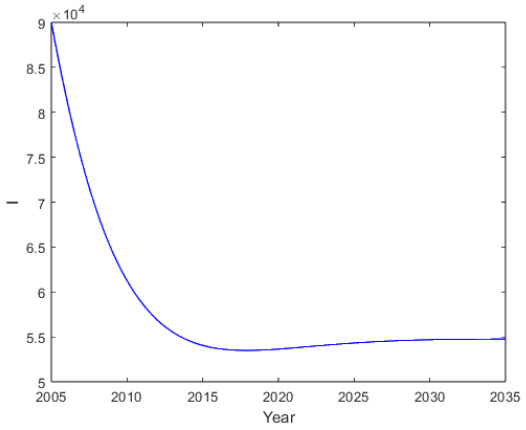

(b)

Figure 3. (a) Review of the current prevalence of brucellosis in Egypt (blue curve: government reports). (b) Prediction of brucellosis infections in Egypt (2005–2025) by the calibrated model.

6. Numerical simulation of optimal control

The correctness of the optimal control theory results and the impact of parameter values on infectious diseases were verified through numerical simulation analysis of the model. Numerical simulations were performed using MATLAB(2021a) software.

Let the state variables be $\mathbf{X} = (S_j, V, S_a, E, I, S_c, W)$,

the costate variables be $\boldsymbol{\lambda} = (\lambda_1, \lambda_2, \lambda_3, \lambda_4, \lambda_5, \lambda_6, \lambda_7)$,

and the control variables be $\mathbf{U}_{ad} = (\mu_1, \mu_2, \mu_3, \mu_4)$.

The basic algorithm steps are as follows:

(1) Make an initial estimation of $\mathbf{U}$ within the time range $[0, t_f]$.

(2) Using the initial conditions and the estimated $\mathbf{U}$ values, solve $\mathbf{X}$ forward in time based on the system (4.1).

(3) Solve the costate variables backward in time using the transversality conditions, control functions, and the values of state variables.

(4) Update $\mathbf{U}$ by inputting the new state variable and costate variable values into the optimal control.

(5) Check for convergence and repeat the above steps until the current state values, adjoint values, and control values converge sufficiently.

The parameter values in Table 3 were adopted as the model's parameter values.

Figure 4 shows the time dynamics of the susceptible adult sheep population S_a, the vaccinated sheep population V, the exposed sheep population E, and the infected sheep population I under both optimal control and no control measures. It deeply reveals the practical effectiveness of the control strategies in mitigating the transmission of brucellosis within the sheep population.

Specifically, Figure 4(a) presents the trajectory of changes in the susceptible adult sheep population S_a. In the absence of any control measures, a sharp decline in S_a can be observed early on, compared with the situation with optimal control. This is because the transmission of the pathogen is unimpeded, leading to a rapid transition of a large number of susceptible adult sheep to the infected state. Although, over time, the disease transmission exhibits a natural weakening trend, this uncontrolled state results in a significant number of sheep dying. These losses not only impose a direct economic burden on farmers, including decreased livestock productivity and increased death-related costs, but also exacerbate the indirect costs caused by the disease's spread to other populations and even humans. In stark contrast, after implementing the optimal control measures, this situation is significantly improved: S_a remains at a higher, stable level for a longer period. This stability indicates that, under control conditions, a large number of sheep can continuously be bred each year, highlighting the critical role of active interventions in protecting the susceptible adult population, which is crucial for maintaining the population's productivity.

Figure 4(b) depicts the dynamic changes in the vaccinated sheep population V. Under the optimal control measures, V shows a clear upward trend. The significant increase in the vaccinated population reflects the successful implementation of the vaccination strategy. This strategy effectively enhances herd immunity by reducing the proportion of susceptible individuals available for infection. Vaccination not only directly protects vaccinated sheep from brucellosis but also indirectly limits the transmission chain by lowering the overall susceptibility of the population. This is a key mechanism for reducing the pathogen's reproduction number R_0. The continued increase in V observed in the controlled scenario further demonstrates that sustained and timely vaccination can establish a robust immune barrier, thereby reducing the risk of large-scale outbreaks.

Figure 4(c) shows the dynamic changes in the exposed sheep population E. The exposed sheep population, representing individuals who have been infected but are not yet infectious, plays a key role in the disease transmission cycle. In the absence of control measures, E increases sharply and significantly because the sheep are continually exposed to infected sheep or contaminated environments (such as shared grazing areas or water sources). The explosive rise in exposed individuals indicates that the number of infected sheep will surge, thereby exacerbating the disease

burden. In contrast, after implementing optimal control measures (such as early detection and isolation of exposed individuals, or disinfection of high-risk environments), E remains at a lower level and ultimately approaches zero. The near elimination of the exposed population highlights the effectiveness of interrupting the transition from exposure to infection, which is crucial for breaking the disease transmission cycle and preventing the disease from becoming entrenched in the population.

Finally, Figure 4(d) focuses on the dynamic changes in the infected sheep population I, the main source of pathogen transmission. In the uncontrolled scenario, I shows an initial exponential growth pattern, which is typical of the disease's spread when it is uncontained, as the pathogen efficiently replicates and spreads among susceptible individuals. In sharp contrast, under optimal control measures, the growth of I is effectively suppressed from the outset, and its curve remains flat and at a low level, indicating that disease transmission is rapidly curtailed.

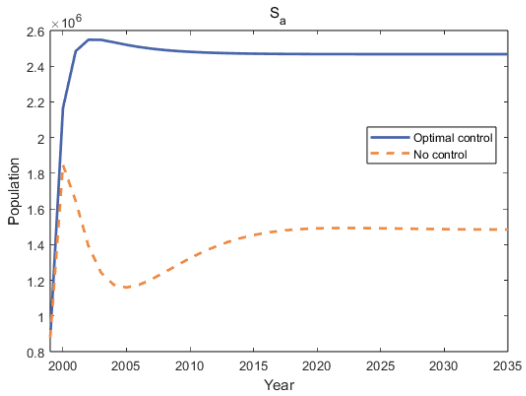

(a) Trajectory of changes in the susceptible adult sheep population S_a.

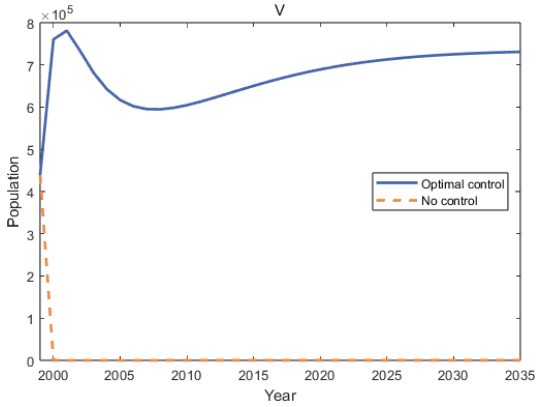

(b) Dynamic changes in the vaccinated sheep population V.

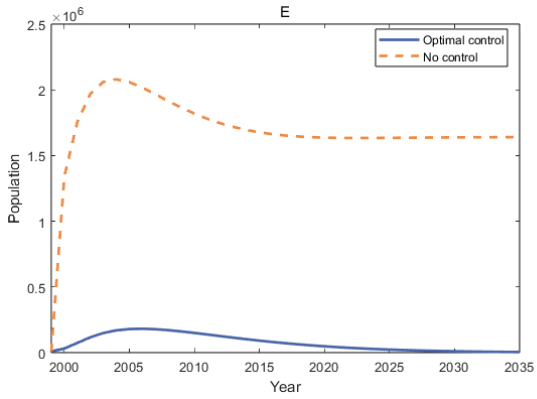

(c) Dynamic changes in the exposed sheep population E.

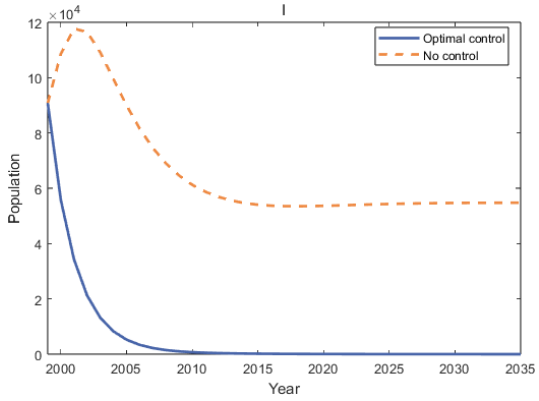

(d) Dynamic changes in the infected sheep population I.

Figure 4. Simulation showing the comparison between optimal control and no control applied.

Overall, the trends presented in Figure 4 highlight the multifaceted effectiveness of optimal control measures in regulating the dynamics of brucellosis. By implementing the strategies we propose, it is

possible not only to alleviate the short-term impacts of the disease but also to contribute to the long-term health and sustainability of the population. Given the zoonotic potential of brucellosis, this is of significant importance for both livestock production and public health.

7. Constant control strategies and cost-benefit analysis

To investigate the impact of different control strategies on prevention and control of the epidemic, we first clarify the design logic of control variable settings in subsequent numerical simulations, addressing concerns about the distinction between constant control and optimal control.

In the analysis of various control strategies (single, dual, triple, and quadruple control) below, the control variables u_1, u_2, u_3, u_4 are set to 0.5. This setting does not represent "optimal control"—a dynamically adjusted strategy derived via Pontryagin's maximum principle presented in Section 6 and Figure 4—but rather serves as a comparative experiment with a constant control intensity. The essence of setting $u_i = 0.5$, where $1 \leq i \leq 4$, is to standardize control effort. Since u_i ranges within $[0, 1]$, 0.5 corresponds to medium-intensity measures such as 50% increases in vaccination coverage or environmental pathogen clearance. This standardization enables a fair comparison of effectiveness across strategy combinations such as single vs. dual strategies under uniform control intensity, intuitively revealing which combinations perform better.

Including constant control simulations is motivated by two key considerations. First, from a practical standpoint, constant measures such as fixed vaccination rates are easier to implement than optimal control, which requires real-time adjustments. Comparing these strategies highlights the superiority of dynamic optimal control while acknowledging the operational simplicity of constant control. Second, the cost-benefit analysis detailed in Table 4 shows that constant strategies—particularly the quadruple control strategy—exhibit higher cost-effectiveness than optimal control, offering a pragmatic policy compromise

Table 4. Comparison of total avoidance, total cost, and unit cost of implementing different control strategies, 1999–2035.

Control strategy	Total number of infections	Total number of infections averted	Total cost (US$)	Unit cost (US$)
No control	2,376,673	–	–	–
Strategy u_2	873,662	1,503,011	1.47×10^9	978
Strategy u_1, u_3	1,642,376	734,297	2.73×10^7	37
Strategy u_1, u_3, u_4	1,597,018	779,655	1.82×10^8	233
Strategy u_1, u_2, u_3, u_4	536,831	1,839,842	1.69×10^9	918
Optimal control	194,640	2,182,033	3.34×10^9	1,531

In summary, simulations with $u_i = 0.5$ serve as a standardized benchmark, facilitating the evaluation of strategy combinations and supporting subsequent cost-benefit analyses and comparisons with optimal control. They enrich our understanding of a strategy's effectiveness under varying implementation frameworks rather than representing optimal control itself.

Beyond optimal control, we propose several alternative control strategies and conduct numerical

simulations on the control the system (4.1) to examine their impacts. To clarify how these strategies influence the progression of brucellosis, we analyze trends in infected sheep populations under different control measures.

The target for control effectiveness is based on relevant guidelines and literature: according to the Ministry of Agriculture and Rural Affairs, "Five-Year Action Program for the Prevention and Control of Inter-Animal Brucellosis (2022–2026)", the target individual positivity rate should remain below 0.4%. However, the literature [31] indicates that brucellosis positivity rates in Egyptian cattle are significantly lower than in sheep, so we aim to reduce the sheep positivity rate to 0.7% or less by 2035. To operationalize this, we calculated the average annual number of Egyptian sheep from 1999 to 2010, multiplied by 0.7%, and set the target for infected individuals to be below 35,000.

Finally, we evaluate all proposed strategies from three perspectives: Total cost, unit cost (ratio of total cost to infections averted), and incremental cost-effectiveness ratio (ICER). The trend of infected individuals under single control measures is specifically shown in Figure 5.

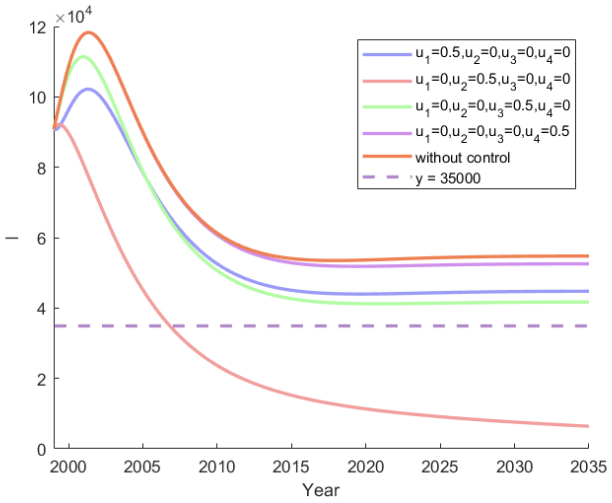

Figure 5. Comparison plot for a single control strategy. The dashed line represents the target we aim to achieve.

It can be observed that without the implementation of relevant control strategies, the number of sheep infected with brucellosis will decrease by 2035 compared with 1999 but will still fall short of our set target. All four control strategies effectively reduce the total number of brucellosis infections in sheep. However, compared with u_1, u_3, and u_4, control strategy u_2 is the most effective in controlling brucellosis infections. It significantly reduces the number of infected sheep and successfully meets our goal, while u_1, u_3, and u_4 also achieve the target we set. Therefore, the single control strategy u_2 is sufficient to reach our goal. Since u_2 alone can achieve the desired outcome, we will not consider it in the subsequent analysis of multiple control strategies.

We now examine the dual control strategies, as shown in Figure 6. It is evident that all three dual control strategies effectively reduce the number of brucellosis infected individuals. Compared with Figure 7, the dual control strategies perform significantly better than the single control strategies, with the exception of u_2. By simultaneously implementing both u_1 and u_3, we can achieve the proposed goal.

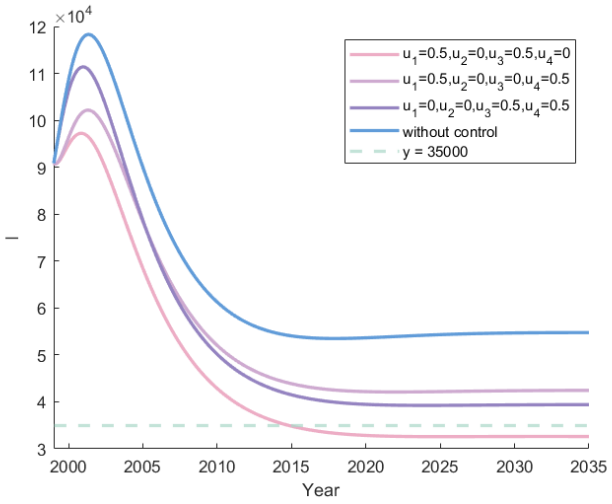

Figure 6. Comparison of dual control strategies. The dashed line represents the target we aim to achieve.

Next, we examine the triple control strategy, as shown in Figure 7. It is evident that the targets set for 2035 can be achieved.

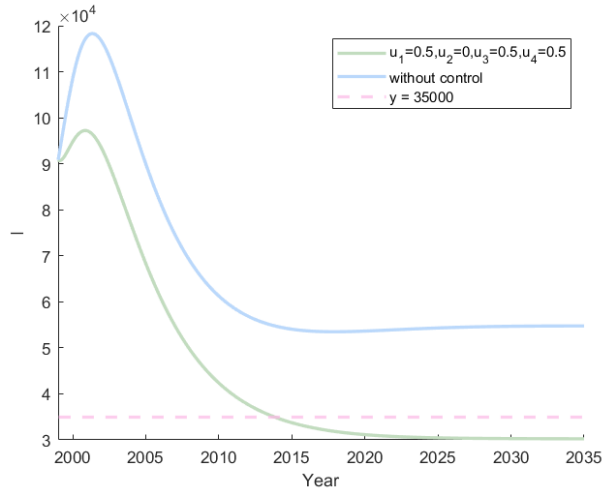

Figure 7. Comparison plot of the triple control strategy. The dotted line represents the target we aim to achieve.

Finally, we examine the quadruple control strategy and the optimal control strategy, as shown in Figures 8 and 9. Both strategies result in an initial rapid reduction in the number of infections, ultimately leading to the elimination of brucellosis. By synthesizing the results from Figures 5–9, we observe that the following strategies all achieve the predefined target: the single control strategy (u_2); the dual control strategy (u_1 and u_3); the triple control strategy (u_1, u_3, and u_4); the quadruple control strategy (u_1, u_2, u_3, and u_4); and the optimal control strategy. Among these, the quadruple control strategy and the optimal control strategy are the most effective in minimizing the number of infections.

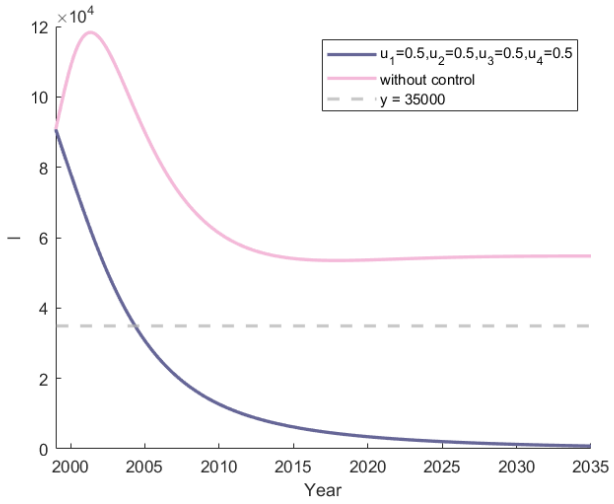

Figure 8. Comparison plot of the four-fold control strategy. The dotted line represents the target we aim to achieve.

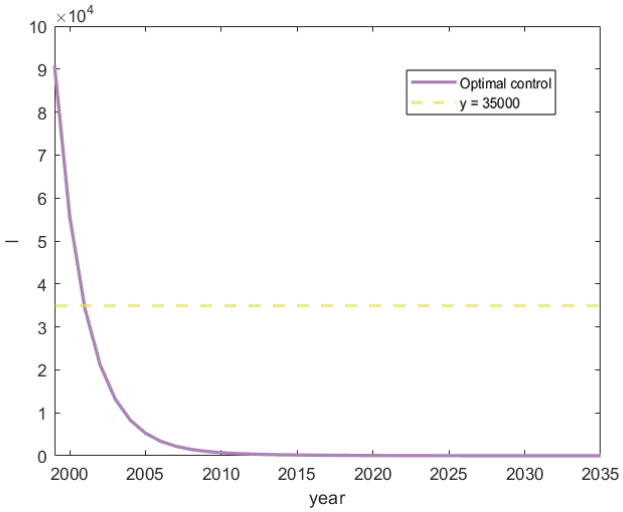

Figure 9. Comparison plot of the optimal re-control strategies. The dashed line represents the target we aim to achieve.

8. Cost-benefit analysis

In this subsection, we conduct a cost-benefit analysis of the control strategies presented in the previous section. We report the total cost of each strategy, the total number of infections averted, and calculate the unit cost for each strategy. Finally, we identify the most cost-effective control method. The total cost is defined as follows:

$$total\ costs = \int_0^{T_0} [\xi_1 u_1 S_j(t) + \xi_2 u_2 (S_a(t) + V(t)) + \xi_3 u_3 V(t) + \xi_4 u_4 (V(t) + W(t))] \mathrm{d}t. \tag{8.1}$$

In the previous subsection, we identified several control strategies that can achieve our proposed goal. Below, we focus on the cost-benefit analysis of these five control strategies, as illustrated in Table 4.

From Table 4, we observe that in terms of the unit cost, the combined strategy u_1, u_3 has the lowest unit cost while still achieving our goal. Therefore, confining and vaccinating young sheep constitutes the most cost-effective approach for disease prevention, despite not completely eliminating brucellosis. In contrast, strategy u_2; the combined strategy u_1, u_2, u_3 and u_4; and the optimal control strategy—though relatively more costly in terms of unit cost—can induce a rapid decline in the number of brucellosis infections and eventually eradicate the pathogen. In the following section, we will employ the ICER to compare these strategies, beginning with the presentation of the ICER expression.

$$\text{ICER} = \frac{C_a - C_b}{I_b - I_a}, \tag{8.2}$$

where C_a and C_b represent the total costs of Strategy a and Strategy b, respectively, and I_a and I_b represent the number of infections under Strategy a and Strategy b, respectively. From its expression we can calculate. Strategy a and Strategy b correspond to any two different prevention and control strategies in Table 4 respectively.

$$ICER(u_1, u_2, u_3, u_3) = 653.15, \quad ICER(\text{optimal control}) = 48218.83. \tag{8.3}$$

It can be observed that the ICER of the optimal control strategy is significantly higher than that of the quadruple control strategy. Therefore, the quadruple control strategy is more cost-effective than the optimal control strategy.

9. Conclusions and discussion

In this paper, we develop an $S_jVS_aEIS_cW$ model for brucellosis with seven compartments, incorporating vaccination, age structure, and environmental contamination. In the theoretical section, we prove that the DFE of the system is globally asymptotically stable when $R_0 \leq 1$. The system is uniformly persistent when the basic reproduction number $R_0 > 1$. Additionally, we derive a theoretical formulation for the optimal control.

In the numerical simulation section, we fit data on the incidence of brucellosis infections in Egyptian sheep from 1999 to 2010 and estimate the model's parameters using the least squares method.

Finally, we perform numerical simulations using the control system developed in the theoretical section to conduct a cost-benefit analysis from the perspective of sheep farmers. Based on real-world conditions, we consider four control strategies: Systematic confinement of young sheep, reducing contact with external sheep and contaminated environments, preventing interaction between immunized adult sheep and external sheep, and improving vaccination coverage while enhancing pathogen clearance from contaminated environments. Our analysis indicates that confining and vaccinating young sheep constitutes the most cost-effective strategy for reducing *Brucella abortus* infections in sheep.

Brucellosis is a disease with extremely complex transmission patterns, affecting individuals of various species including cattle, sheep, and dogs. In this paper, we only discuss the transmission of brucellosis in sheep. Due to the complexity of the model, we do not consider the possibility of

co-infections with other organisms. However, there are already many studies in the existing literature that explore brucellosis transmission across multiple populations, and our model can still be applied to other organisms. Compared with existing models, our model takes vaccination, contaminated environments, and age structure into account. Nevertheless, due to the complexity of its transmission patterns, it is difficult to comprehensively consider all aspects of its epidemiology. For example, our data are annual, which overlook the differences in the reproductive capacity of sheep across different seasons of the year.

In summary, we developed a seven-compartment brucellosis model that integrates vaccination, age structure, and environmental contamination. We analyzed its dynamic behavior, calibrated the model using empirical data, and proposed a set of control strategies along with cost-benefit analyses. Although our study focuses on a specific sheep population, the model is applicable to brucellosis in other species worldwide.

Use of AI tools declaration

The authors declare they have not used Artificial Intelligence (AI) tools in the creation of this article.

Acknowledgments

This work was supported by Science and Technology Development Plan Project of Jilin Province, China (No. 20230101291JC) and China Scholarship Council (No. 201807585008).

Conflict of interest

The authors declare there is no conflict of interest.

References

1. D. Shang, D. Xiao, J. Yin, Epidemiology and control of brucellosis in China, *Vet. Microbiol.*, **90** (2002), 165–182. https://doi.org/10.1016/s0378-1135(02)00252-3
2. J. González-Guzmán, R. Naulin, Analysis of a model of bovine brucellosis using singular perturbations, *J. Math. Biol.*, **33** (1994), 211–223. https://doi.org/10.1007/BF00160180
3. J. Nie, G. Sun, X. Sun, J. Zhang, N. Wang, Y. Wang, et al., Modeling the transmission dynamics of dairy cattle brucellosis in Jilin Province, China, *J. Biol. Syst.*, **22** (2014), 533–554. https://doi.org/10.1142/S021833901450020X
4. J. Zhang, G. Sun, X. Sun, Q. Hou, M. Li, B. Huang, et al., Prediction and control of brucellosis transmission of dairy cattle in Zhejiang Province, China, *PLoS ONE*, **9** (2014), 108592. https://doi.org/10.1371/journal.pone.0108592
5. G. Sun, Z. Zhang, Global stability for a sheep brucellosis model with immigration, *Appl. Math. Comput.*, **246** (2014), 336–345. https://doi.org/10.1016/j.amc.2014.08.028
6. Q. Hou, Global analysis of a multi-group animal epidemic model with indirect infection and time delay, *J. Appl. Anal. Comput.*, **6** (2016), 1023–1040. https://doi.org/10.11948/2016066

7. P. O. Lolika, S. Mushayabasa, C. P. Bhunu, C. Modnak, J. Wang, Modeling and analyzing the effects of seasonality on brucellosis infection, *Chaos Solitons Fractals*, **104** (2017), 338–349. https://doi.org/10.1016/j.chaos.2017.08.027
8. L. Zhou, M. Fan, Q. Hou, Z. Jin, X. Sun, Transmission dynamics and optimal control of brucellosis in Inner Mongolia of China, *Math. Biosci. Eng.*, **15** (2018), 543–567. https://doi.org/10.3934/mbe.2018025
9. Q. Hou, X. Sun, Modeling sheep brucellosis transmission with a multi-stage model in Changling County of Jilin Province, China, *J. Appl. Math. Comput.*, **51** (2016), 227–244. https://doi.org/10.1007/s12190-015-0901-y
10. Q. Hou, X. Sun, J. Zhang, Y. Liu, Y. Wang, Z. Jin, Modeling the transmission dynamics of sheep brucellosis in Inner Mongolia Autonomous Region, China, *Math. Biosci.*, **242** (2013), 51–58. https://doi.org/10.1016/j.mbs.2012.11.012
11. C. Yang, P. O. Lolika, S. Mushayabasa, J. Wang, Modeling the spatiotemporal variations in brucellosis transmission, *Nonlinear Anal. Real World Appl.*, **38** (2017), 49–67. https://doi.org/10.1016/j.nonrwa.2017.04.006
12. M. Li, G. Sun, Y. Wu, J. Zhang, Z. Jin, Transmission dynamics of a multi-group brucellosis model with mixed cross infection in public farm, *Appl. Math. Comput.*, **237** (2014), 582–594. https://doi.org/10.1016/j.amc.2014.03.094
13. B. Aïnseba, C. Benosman, P. Magal, A model for ovine Brucellosis incorporating direct and indirect transmission, *J. Biol. Dyn.*, **4** (2010), 2–11. https://doi.org/10.1080/17513750903171688
14. C. Li, Z. Guo, Z. Zhang, Transmission dynamics of a brucellosis model: Basic reproduction number and global analysis, *Chaos Solitons Fractals*, **104** (2017), 161–172. https://doi.org/10.1016/j.chaos.2017.08.013
15. K. Meng, X. Abdurahman, Study of the brucellosis transmission with multi-stage, *Commun. Math. Biol. Neurosci.*, **2018** (2018), 20. https://doi.org/10.28919/cmbn/3796
16. J. Zinsstag, F. Roth, D. Orkhon, G. Chimed-Ochir, M. Nansalmaa, J. Kolar, et al., A model of animal-human brucellosis transmission in Mongolia, *Prev. Vet. Med.*, **69** (2005), 77–95. https://doi.org/10.1016/j.prevetmed.2005.01.017
17. M. Li, G. Sun, J. Zhang, Z. Jin, X. Sun, Y. Wang, et al., Transmission dynamics and control for a brucellosis model in Hinggan League of Inner Mongolia, China, *Math. Biosci. Eng.*, **11** (2014), 1115–1137. https://doi.org/10.3934/mbe.2014.11.1115
18. H. R. Holt, M. Walker, W. Beauvais, P. Kaur, J. S. Bedi, P. Mangtani, et al., Modelling the control of bovine brucellosis in India, *J. R. Soc. Interface*, **20** (2023), 20220756. https://doi.org/10.1098/rsif.2022.0756
19. W. Wang, X. Abdurahman, Dynamics of a stochastic multi-stage sheep brucellosis model with incomplete immunity, *Int. J. Biomath.*, **16** (2023), 08. https://doi.org/10.1142/S1793524522501388
20. L. Zhou, M. Fan, Q. Hou, Z. Jin, X. Sun, Transmission dynamics and optimal control of brucellosis in Inner Mongolia of China, *Math. Biosci. Eng.*, **15** (2018), 543–567. https://doi.org/10.3934/mbe.2018025

21. B. Nannyonga, G. G. Mwanga, L. S. Luboobi, An optimal control problem for ovine brucellosis with culling, *J. Biol. Dyn.*, **9** (2015), 198–214. https://doi.org/10.1080/17513758.2015.1056845
22. H. Khalil, *Nonlinear Systems*, Prentice Hall, 3^{rd} edition, 2002.
23. O. Diekmann, J. A. P. Heesterbeek, J. A. J. Metz, On the definition and the computation of the basic reproduction ratio R_0 in models for infectious diseases in heterogeneous populations, *J. Math. Biol.*, **28** (1990), 365–382. https://doi.org/10.1007/BF00178324
24. P. van den Driessche, J. Watmough, Reproduction numbers and sub-threshold endemic equilibria for compartmental models of disease transmission, *Math. Biosci.*, **180** (2002), 29–48. https://doi.org/10.1016/s0025-5564(02)00108-6
25. J. P. La Salle, *The Stability of Dynamical Systems*, Society for Industrial and Applied Mathematics, 1976. https://doi.org/10.1137/1.9781611970432
26. X. Zhao, *Dynamical Systems in Population Biology*, Spring, 2^{nd} edition, 2017. https://doi.org/10.1007/978-3-319-56433-3
27. R. A. Horn, C. R. Johnson, *Matrix Analysis*, Cambridge University Press, 2012. https://doi.org/10.1017/CBO9780511810817
28. W. Wang, X. Zhao, An epidemic model in a patchy environment, *Math. Biosci.*, **190** (2004), 97–112. https://doi.org/10.1016/j.mbs.2002.11.001
29. O. Diekmann, J. A. P. Heesterbeek, M. G. Roberts, The construction of next-generation matrices for compartmental epidemic models, *J. R. Soc. Interface*, **7** (2010), 873–885. https://doi.org/10.1098/rsif.2009.0386
30. Z. Yue, Y. Mu, K. Yu, Dynamic analysis of sheep Brucellosis model with environmental infection pathways, *Math. Biosci. Eng.*, **20** (2023), 11688–11712. https://doi.org/10.3934/mbe.2023520
31. G. Wareth, A. Hikal, M. Refai, F. Melzer, U. Roesler, H. Neubauer, Animal brucellosis in Egypt, *J. Infect. Dev. Countries*, **8** (2014), 1365–1373.
32. A. M. S. Menshawy, A. F. Vicente, Y. M. Hegazy, V. Djokic, M. E. R. Hamdy, L. Freddi, et al., Animal brucellosis in Egypt: Review on evolution, epidemiological situation, prevalent brucella strains, genetic diversity, and assessment of implemented national control measures, *Microorganisms*, **13** (2025), 170. https://doi.org/10.3390/microorganisms13010170

AIMS Press